R-99-67

DECOVALEX II project

Nirex RCF Shaft Excavation Task 1C – Coupled hydro-mechanical effects of shaft sinking within Sector 7

Hossein Hakami

Itasca Geomekanik AB

December 1999

Svensk Kärnbränslehantering AB
Swedish Nuclear Fuel
and Waste Management Co
Box 5864
SE-102 40 Stockholm Sweden
Tel 08-459 84 00
+46 8 459 84 00
Fax 08-661 57 19
+46 8 661 57 19

ISSN 1402-3091
SKB Rapport R-99-67

DECOVALEX II project

Nirex RCF Shaft Excavation Task 1C – Coupled hydro-mechanical effects of shaft sinking within Sector 7

Hossein Hakami

Itasca Geomekanik AB

December 1999

Keywords: DECOVALEX, Numerical Modelling, *FLAC*^{3D}, Shaft Sinking

Executive Summary

Within the framework for an international co-operation in the field of geohydrological and mechanical processes associated with radioactive waste disposal deep in rock masses (DECOVALEXII), the present work involved a number of numerical investigations in order to gain an understanding of the consequences a shaft sinking at Sellafiled, England, may bring about.

Research groups from five countries, namely Finland, France, Japan, Spain and Sweden approached the modelling of the shaft sinking in the rock mass in question with different numerical methods. Both continuum as well as discontinuum representations of the rock mass were made. Itasca chose the code *FLAC*^{3D}, a three dimensional finite difference based computer code to carry out the numerical analyses necessary.

As a first approach, an equivalent material model was chosen where discontinuities at all levels assumed to have smeared out in a rock matrix, to produce a theoretical material that would behave elasto-plastically under loading. By selecting the Mohr-Coulomb failure criterion, numerical analyses were carried out that depicted the perturbations in stress and deformational field, the shaft sinking would produce.

The sinking of the shaft disturbs the flow regime of the rock mass. By presuming a number of assumptions, the approximate discharge into selected sections of the shaft were computed. Also, by numerically "monitoring" the pore pressure drawdowns in two boreholes in close vicinity of the shaft the effect of the shaft sinking on the flow was evaluated.

Having evaluated the outcome of the first series of the numerical analyses, improvements were made in the model set-up, by introducing three major flow zones with enhanced porosity and permeability in a grid that was otherwise a low conductive medium with very low porosity. A new set of flow analyses were carried out that typified the effect of the added flow zones on the general characteristics of flow in the rock mass in question. Also, by introducing a new failure criterion - emerged from both Mohr-Coulomb and Hoek&Brown failure criteria - that takes care of the onset of a brittle failure more explicitly, numerical analyses were carried out in order to capture the Excavation Damage Zone, a feature that could not be studied under the failure criterion and the input data incorporated in the first modelling approach.

Regardless of which of the two failure criteria was active in the simulations, the deformational disturbances caused by the numerical excavation of the shaft were typical for stiff and competent crystalline rock masses. The mechanically disturbed zone did not effectively extend farther than about three times the diameter of the shaft, beyond which the disturbance was insignificant. Also, the convergence of the shaft was confined to about 3 mm at the most, once again typical for the hard rocks.

As was expected, there was a very significant difference in flow characteristics associated with the two model set-ups; with and without the outstanding flow zones.

While both the modelled rock matrices had almost similar flow properties, the flow zones only appearing in the second model were supplied with uppermost values of the permeability and porosity from ranges estimated from the site and laboratory investigations. The extreme values were between x – y order of magnitudes greater than the corresponding values from the rock matrix.

Extremely low volumes of water, up to about 2.5 lit/min percolated into a 20-m long section of the shaft, by using the first model set-up with no flow zones included. On the other hand much greater values; e.g. as high as about 260 lit/min flowed into the same section of the shaft, having the three flow zones active. The latter case may be considered as a possible upper bound for the inflow into the shaft over a section of 20 meters long that may take place.

An Excavation Damage Zone was numerically captured that extended, at certain points, to about 60 centimetres into the rock from the shaft walls. The thickness of the damaged zone is clearly dependent on the fineness with which the grid zones were discretized. A rough comparison between the 60 cm thickness of the EDZ detected numerically and that normally estimated from *in-situ* investigations of the zone around openings in similar hard rocks served as an indication of the appropriateness of the discretization used in the model set-up.

Contents

List of Figures

1 Introduction

1.1 Background

In 1992 scientists from eight countries joined together in order to establish an international project that would enhance the existing knowledge in the field of coupled thermo, hydrogeological and mechanical processes that take place within a rock mass because of the emplacement of waste radioactive fuel.

The project was entitled as the Development of Coupled thermo hydro-mechanical models and their Validation against Experiments, shortened in title as DECOVALEX. National governmental agencies responsible for radioactive waste isolation supported the project financially and participated in works related to administration as well as in scientific issues of concern.

The time length of the project was chosen to be four years, from 1992 to 1996. The Swedish Nuclear Power Inspectorate (SKI) was responsible for the management of the project.

A second phase of the project started directly following the first phase, whereupon a time span of about three years (1996 to 1998) was allocated to this phase to complete; and was named as DECOVALEX II Project. The nature of the work was different from the first phase in that the research teams were divided into two groups in order to tackle two ongoing projects through numerical analyses. The projects are the Kamaishi Mine in-situ experiment in Japan and the shaft sinking investigations at Sellafield in England.

1.2 Present work

The present work covers partly the investigations in form of numerical analyses related to Sellafield shaft sinking project: Task 1 Nirex RCF Shaft Excavation. The investigations reported here were carried out under the final section of the Task 1 project, namely Task 1C.

Being titled as : Coupled hydro-mechanical effects of shaft sinking within sector 7, Task 1C is the final sub-task of a set of three consecutive sub-tasks, the first two of which were named as Task 1A and Task 1B. Both Task 1A and Task 1B have already been carried out and reported, see Israelsson 1997 and 1996.

Task 1A involved efforts expended in order to numerically simulate a comprehensive pumping test that was performed inside RCF3 borehole at Sellafield. Simulations performed were aimed to explore the capability and flexibility a variety of numerical

methods would exhibit in order to simulate the rock mass in question and to try to capture the pumping test results. Different codes used required that the rock mass would be modelled in accordance with the features each code possessed. Not much effort was made at this level to enhance the simulated results as regards their closeness to the real in-situ data.

Having examined the codes in the manner mentioned above, it was then pertinent to initiate a new phase (Task 1B) where the models already set up should be calibrated against some relevant field measurements. Alternatively the models should be improved in order to achieve results closer to the field measurements.

Works initiated under Task 1C were aimed to sketch an image of the consequences the sinking of the planned shaft at Sellafield would bring about. Investigations carried out under Task 1A and Task 1B made bases on which simulation works related to Task 1C should be placed.

Not only the hydrogeological perturbations of the shaft sinking, but also the mechanical disturbances in conjunction with the excavation works were to be investigated. Because of the function of the shaft, the investigations included both far-field as well as near-field scales.

1.3 Framework for Task 1C

Based on the comprehensive site investigations that were performed at Sellafield, a concise document was worked out (Stephansson and Knight, 1997) that provided an adequate minimum of site and laboratory measurement results needed to set up the computational models in their initial rough forms. The document also provided guidelines and patterns for how the simulation findings should be planned and presented. The follow-up of the document would serve in uniforming the findings of the different research teams and facilitates the comparisons.

The first draft of the document was released on July 7, 1997. The research teams and the funding organisations submitted their view points on the document later and the amended document was made available on September 18, 1997. Itasca Geomekanik AB was awarded a contract from Swedish Nuclear Waste Mangement company (SKB) to work on Task 1C on October 23, 1997.

Research teams reported on their progress during a workshop held in Berkeley, California during December 8 – 10, 1997.

Following a Task Force meeting held at NIREX offices in Oxfordshire.

On March 31, 1998, the research teams presented their latest results in Avignon, France during June 15 – 19, 1998, and were encouraged to finalize their works and to prepare a draft for the final report not later than the end of November - beginning of December 1998.

For the simplicity of referring to the two subsequent parts of the investigations that was carried out and presented at Berkeley and Avignon, the models are referred to as the "Berkeley" model and the "Avignon" model in this report.

2 Site geology

The Sellafield site is located on the north-western coast of Great Britain in the Cumbria district. NIREX has been characterizing the Sellafield site since 1989 to determine whether it is suitable for disposal of low and intermediate radioactive waste in a deep repository. The Potential Repository Zone identified by NIREX is located 3 km inland from the Sellafield works at a depth of approximately 650 m bOD (below Ordnance Datum – i.e., below mean sea level) in the volcano-clastic rock of the Borrowdale Volcanic Group (BVG). The BVG is overlain by a sedimentary breccia, known as the Brockram, approximately 70-80 m thick. Above the Brockram, there is a sandstone group. Two cross sections of the Potential Repository Zone are shown on Figures 2-1 and 2-2.

The ground surface dips gently toward the sea and some kilometers inland; the mountains of Cumbria have peaks close to 1000 m above sea level. The site has been characterized by core logging from both deep and shallow boreholes, seismic studies , hydrogeological and geochemical investigations and long-term hydrogeological monitoring.

The Borrowdale Volcanic Group consists of metamorphosed volcanic rocks that are fractured at all scales (NIREX, 1993). The BVG succession is dominated by thick sheets of pyroclastic rocks, interpreted mostly as ignimbrite. Most of the the thick ignimbrites of the BVG are compound sheets comprising multiple flaws with complex facies distribution of lithologies, welding and primary alteration profiles. Poorly sorted volcanic breccias are associated with the basal section of individual ignimbrite sheets. The spacing and the nature of flow zones in the BVG indicate that the rock mass may have experienced several stages of fracturing (NIREX, 1995).

Most of the BVG is inferred to be high quality rock associated with Dynamic Rock Quality Index (DRQI) values of M1, M2 and M3, see Table 2-1. Most of the anomalous zones of inferred low rock quality within the BVG can be associated with faulting. Also, both silicic alteration zone within the Longlands Farm Member and the Sides Farm member are zones of relatively lower quality rock.

The Longlands Farm Member in the RCF South shaft boreholes can be subdivided into three predominant rock quality intervals on the basis of DRQI (Table 2-1). The upper interval is very variable, contains the mesobreccia and is characterised by M2, the middle interval coincides with the intensely altered zone and is characterised predominantly by strongly anomalous M5 and M8 DRQI divisions. The lower interval contains mostly M1 to M3 divisions characteristic of the BVG in general, but is predominantly characterised by M1.

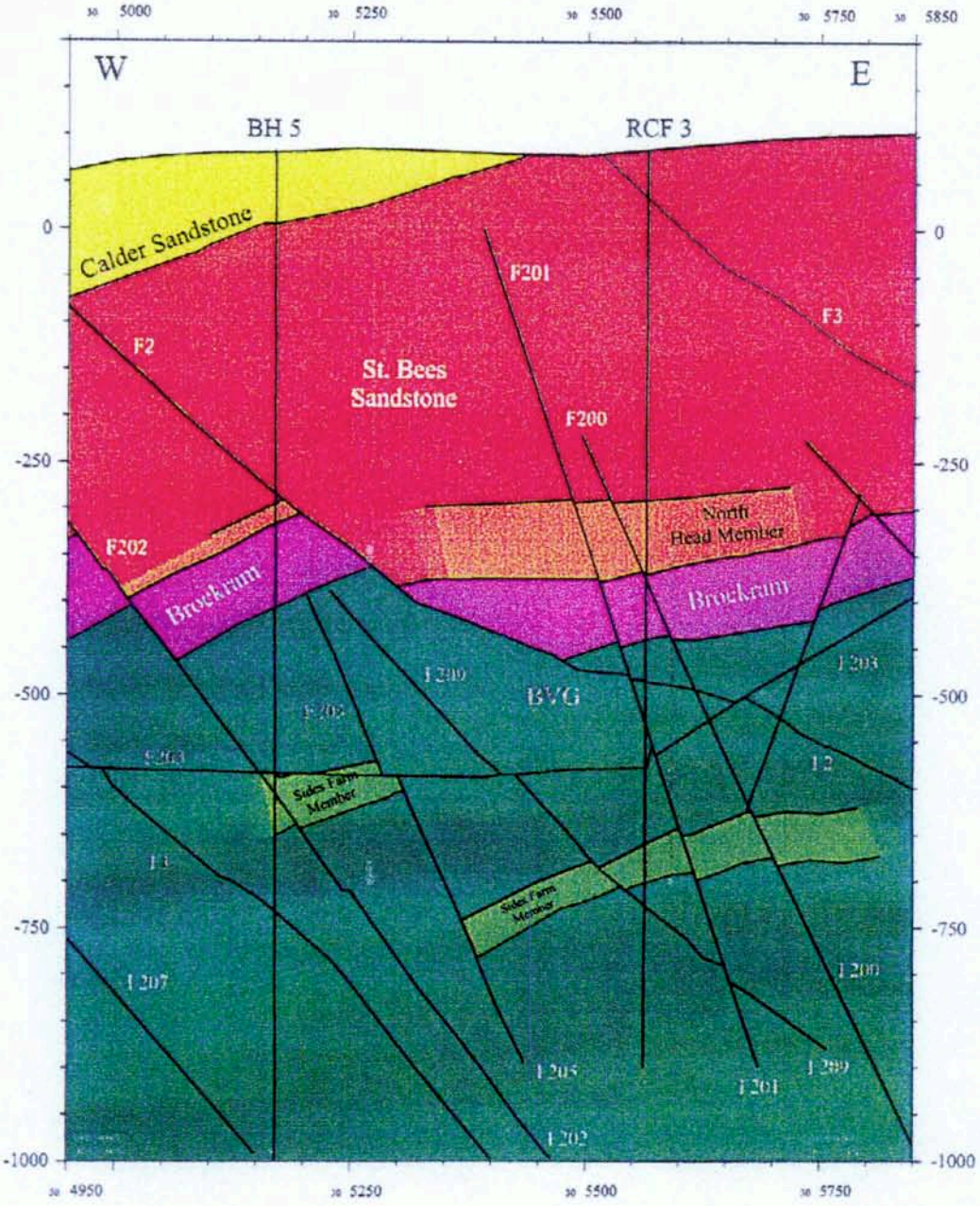

Figure 2-1 W-E orientated geological cross-section of the Potential Repository Zone.

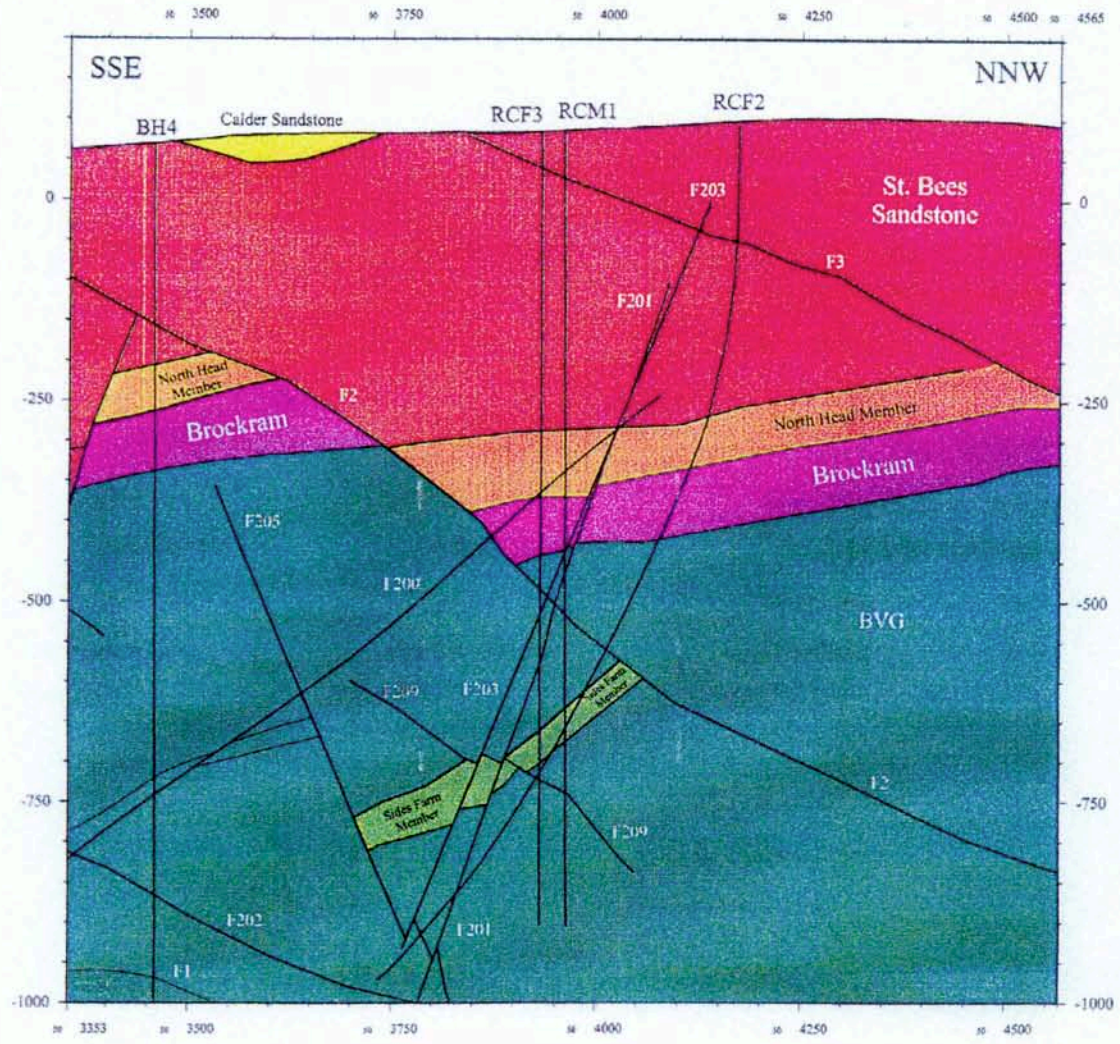

Figure 2-2 SSE-NNW oriented geological cross-section of the potential Repository Zone.

It has been found out that the ground water flow in the BVG takes place predominantly through networks of connected fractures (Armitage et al., 1995). Further, significant flow has been observed to occur in a limited number ofthe so called flow zones.

Table 2-1 DRQI intervals and associated response parameters for the RCF South Shaft boreholes (after Science report, NIREX, 1995)

DRQI interval	Shear Modulus (Gpa)	Bulk Modulus (Gpa)	Young's Modulus (GPa)
M1	32	59	82
M2	27	53	70
M3	24	46	62
M4	20	38	52
M5	18	33	45
M6	14	22	35
M7	10	19	26
M8	16	42	44

Table 2-2 Ground water flow distribution in the sandstone, Brockram and the BVG.

Features in BH 2, 5, 11, 14, RCF1, 2, 3, RCM1, RCM2, RCM3	Sandstone	Brockram	BVG
Flow through permeable rock matrix	85%	36%	0%
Flow through faults	0%	50%	20%
Flow associated with planar fractures coated by earthy hematite	1%	0%	20%
Flow associated with late, steep, dilatational, open or vuggy veins	14%	14%	61%

Most of the flow zones consist of a number of fractures that carry water. Temperature and electrical conductivity measurements identified 20 flow zones within 1140 m ofthe BVG in Borehole 2, nine zones within 850 m in Borehole 4 and eight zones within 770 m in borehole 5, see Figure 2-1 and 2-2 and Figure 2-3 for the position of the boreholes. The rock between these flow zones is observed to be fractured, with natural open fractures occurring at a spacing of approximately one meter along the borehole axis. It is expected that such fractures do conduct water, but the transimissivities are too low to be detectable by production logging. The rock between the fractures has a low permeability (Armitage et al., 1995).

Preliminary analyses suggest that flow in the boreholes is associated with the four types of features listed in Table 2-2 (Knight, 1996).

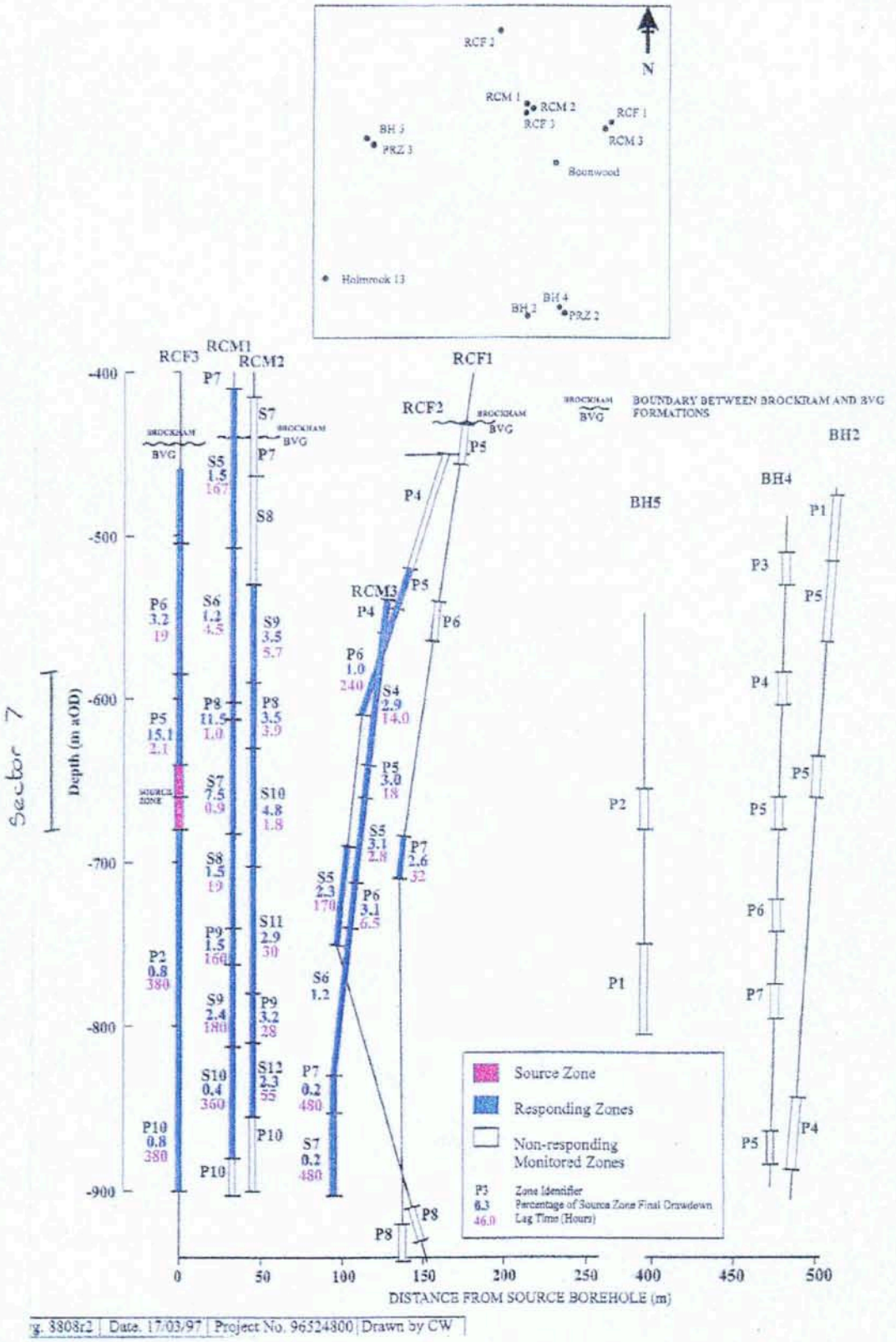

Figure 2-3 Illustration of the relationship of Sector 7 in RCF3 to adjacent monitoring zones.

3 Field data

Based on agreements reached, NIREX provided each research team working on Task 1 with a complete set of documents, which had been worked out based on extensive site investigations at Sellafield and laboratory experiments. Later in June 1997, when Task 1C was discussed and decided upon, a short and concise document was made available entitled as "DECOVALEX II Project, Task 1C coupled hydro-mechanical effects of shaft sinking within Sector 7 (Stephansson and JL Knight, 1997), in which a minimum necessary set of data were compiled in order that the research teams would more readily select those input parameters needed for their numerical analyses.

An extract of the content of the document mentioned above is given below that typifies the rock mass in question.

3.1 In-situ stresses

According to NIREX, the in-situ state of stress at the site in question is defined by the following relationships:

$$\sigma_v = (0.02494 \pm 0.00025)D + (0.26622 \pm 0.25326) \text{ MPa} \quad 3\text{-}1$$

$$\sigma_{Hmin} = (0.01996 \pm 0.00113)D - (0.31619 \pm 1.15545) \text{ MPa} \quad 3\text{-}2$$

$$\sigma_{Hmax} = (0.03113 \pm 0.00227)D + (1.88747 \pm 2.284202) \text{ MPa} \quad 3\text{-}3$$

Where D is depth in meter from the Ordnance datum that occurs 100 meters below the ground surface. The orientation of σ_{Hmax} is 340° from North.

Using the above relations, the principal in-situ stresses were calculated for the depth range of 425 –720 meter, over which the mechanical computations for the Berkeley model (see chapter 4) were performed. The corresponding ranges for σ_v, σ_{Hmin} , σ_{Hmax} , become 13. 4 – 20.7 MPa, 10.2 – 16.1 MPa and 18.2 – 27.4 MPa respectively. Note that the σ_{Hmax} and the σ_{Hmin} occur to be the Major and the minor principal stress respectively.

3.2 Rock mass properties

Table 3-1 lists the rock material parameters found for the BVGthat are based on rock sample laboratory tests, and Table 3-2 lists the rock material properties estimated by seismic methods.

Four major fracture sets have been distinguished at the site. Data on their orientation, spacing and residual friction angles are given in Table 3-3.

Deduced rock mass parameters are listed in Table 3-4.

Table 3-1 Rock material properties determined by laboratory tests.

Core data	Maximum	Minimum	Mean value
Uniaxial compressive strength (MPa)	308.8	29.1	157.0
Young's Modulus (GPa)	97.50	73.80	84.60
Poisson's Ratio	0.25	0.22	0.24
Effective Porosity (%)	4.53	0.05	0.86
Saturated Density (Mg/m3)	2.92	2.66	2.75
Hoek&Brown m value	9.78	3.171	7.453
Hoek&Brown s value	1.71	0.63	1.062
Apparent cohesion of intact rock from triaxial test (MPa)	56.55	11.32	30.0

Table 3-2 Rock mass properties estimated by seismic methods.

Wireline Data	Maximum	Minimum	Mean value
Young's modulus (GPa)	99.56	31.17	69.08
Poisson's Ratio	0.354	0.168	0.263
Porosity (%)	12.66	0.01	5.19
Bulk density (Mg/m^3)	2.82	2.58	2.69
Compressional Sonic velocity (km/s)	6.59	3.89	5.60
Shear Sonic velocity (km/s)	3.84	2.11	3.18

Table 3-3 Fracture data from the dominant four fracture sets within the Potential repository Zone.

Set Number	Mean Dip/Dip direction(°)	Max/Min Spacing(m)	Mean Spacing(m)	Residual angle of Friction(°)
Set 1	08/145	5.35/0	0.29	24.9
Set 2	88/148	2.21/0	2.21/0	28.0
Set 3	76/021	2.01/0	0.28	27.0
Set 4	69/087	3.54/0	0.31	31.0

Table 3-4 Parameters characterizing the rock mass at the site.

Parameter	Interpreted	Maximum	Minimum
Q-index	44.55		
RMR rating	71.79		
Hoek&Brown m value	6.21		
Hoek&Brown s value	0.04		
E_{mass} (GPa)	65.0		
Hydraulic conductivity (m/s)		$10^{-6.69}$	$10^{-10.92}$

4 The Berkeley model

4.1 Preface

As was mentioned in section 1.2, Task 1C involves numerical analyses that would predict consequences a shaft sinking may bring about given a site with the geological characteristics outlined in previous chapters.

To begin with, it was assumed that the rock mass would behave in a continuous manner. An "equivalent" material model that smears out the discontinuities into a rock matrix could then be adopted to fit into the continuum formulations.

$FLAC^{3D}$, a three dimensional finite difference-based code (Itasca, 1998) was then selected as the tool for the numerical analyses.

4.2 The grid

Having adopted to represent the rock mass as a continuum, where the rock discontinuous features were not modelled explicitly, rather an equivalent material model represents the fractured rock, it was possible to take benefit of symmetry planes in order to reduce the overall size of the model.

By using two symmetry planes, a quadratic prism was built to represent one fourth of the rock mass volume chosen to be included in the analyses. The size of the block was 264 m × 264 m × 377.5 m, which meant that a block of the rock mass with dimensions of 528 m × 528 m × 377.5 m was included in the computations.

The upper side of the model block was taken to lie at the depth of 425-meter boD, to roughly coincide with the bottom of the Brockram formation. No part of the overlying sandstone that borders with the Brockram formation was therefore included in the model block.

In $FLAC^{3D}$, the bulk of the model block is constructed by adding large "bricks" (named as primitives in $FLAC^{3D}$) that are shaped differently. Each primitive is then discretized into a number of minor grid zones; the grid zones are not normally identical in shape within a single primitive and/or in between neighbouring primitives.

One single primitive as described above could construct the model block. However, because of the requirements to collect data at predetermined points, it necessitated building up the model block by unsimilar primitives that have differently shaped grid zones. In this way the data collecting points either coincided with grid points or lied in

the close vicinity of grid points or grid zone centroids. In $FLAC^{3D}$, computed parameters may be readily picked up at grid points or at the centroid of each grid zone. In this way no interpolation of data between grid points seemed necessary. Figure 4-1 shows the model block built up by adding different primitives. It contained about 7000 grid zones.

As opposed to the mechanical computations, the hydrogeological computations need a larger model block. By adding primitives at the bottom of the model block, it could be enlarged to suit the hydrogeological computations. The larger grid that was built in this way, had the bottom at 802.5 m boD and included a block of the rock mass with dimensions of 528 × 528 × 802.5 meter in computations. The number of grid zones increased, as a result, to about 9000.

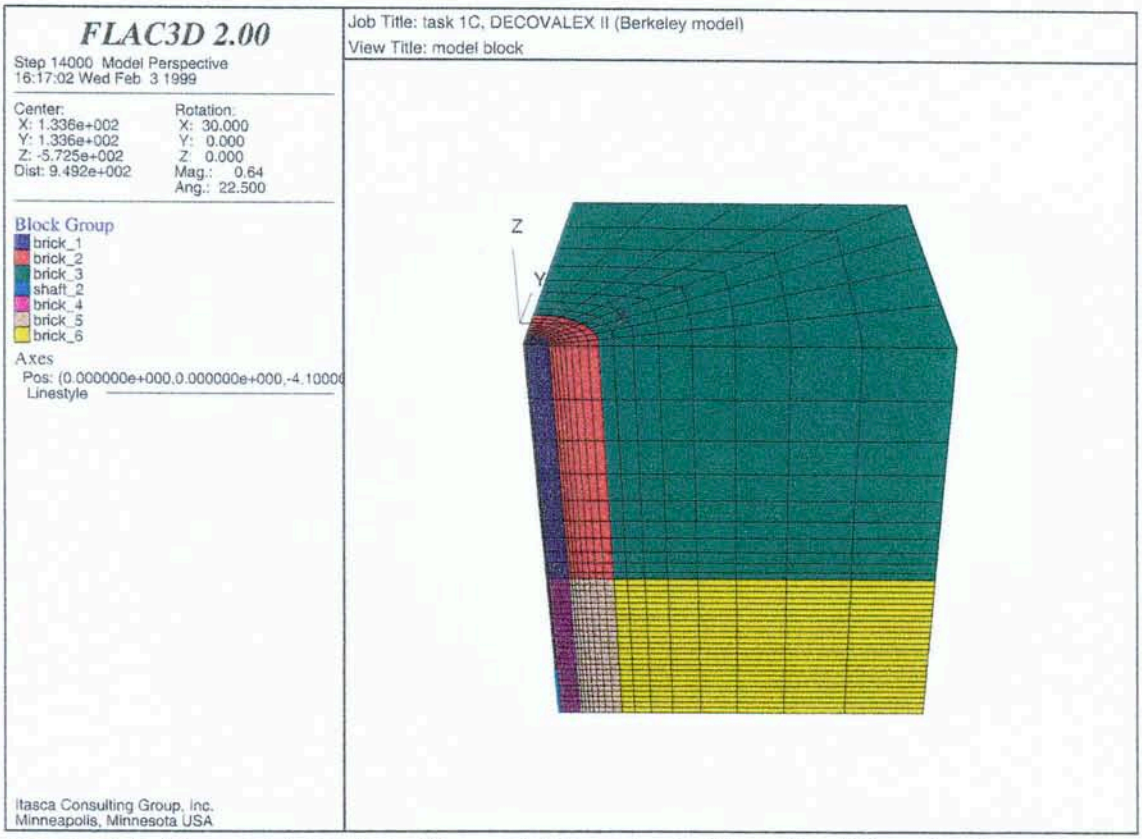

Figure 4-1 The model block, built up of different primitives (in different colours in order to bring grid points closer the to the predefined data collection points.

4.3 Mechanical computations

4.3.1 Boundary conditions

As the mechanical disturbances due to the shaft sinking were not expected to extend beyond a limited number of meters from the shaft walls and bottom, the model boundaries, excluding the top of the model, were simply chosen to be as if no displacement of the rock, perpendicular to the boundaries, and in that vicinity, would take place. The top of the model block was loaded by a vertical stress that corresponded to σ_v at that depth.

4.3.2 Mechanical properties

The mechanical parameters needed to set up the model were extracted from NIREX protocol regarding Task 1C and are listed in Table 4-1 below:

Table 4-1 Mechanical properties of the rock mass Boundary conditions

Parameter	Magnitude
Interpreted E_{mass}	65 GPa
Poisson ratio	0.24
Angle of internal friction	35
Cohesion	11.3 MPa
Tensile strength$_{(mass)}$	1 MPa

The chosen tensile strength of the rock mass is just an arbitrary low value. No information on the tensile strength of the rock mass in question was provided by NIREX. It is, however, well understood that rock masses exhibit no or very little resistance against tensile forces. The low value chosen assures that the rock mass is modelled such as not to tolerate any tensile stresses exceeding 1MPa.

The rock mass was modelled as linearly elastic, perfectly plastic material with a failure surface defined by the Mohr-Coulomb criterion.

4.3.3 The sequence of computations

According to the construction plans, the shaft was to be excavated at an advance rate of 1.25 meter per day, i.e., a blast round of 2.5-meter length should take two days to excavate. Sector 7, the 40-meter stretch of the shaft between 640 – 680 meter deep would, accordingly, require 16 blast rounds to complete.

For the mechanical computations, Sector 7 was numerically "excavated" in eight, 5-meter thick intervals instead of 16. Otherwise the results and the computation time would have increased excessively. Also, the upper stretch of the shaft, between 425 and 640 meters of depth was numerically excavated in two sections, rather than in several blast rounds of 5 meters advance. No measurements from this stretch were expected to be collected, and any influence from this stretch on the mechanical disturbances associated with Sector 7 was judged to be marginal.

The model was run to equilibrium for each section of the shaft excavated. It was controlled that no further changes in deformations or stresses took place by running the model further, beyond the state that was nominally taken to represent the apparent steady state.

4.3.4 Results

The contours of displacement on vertical planes through Diagonal1(azimuth N340°) and Diagonal 3(azimuth N70°) are given in Figures 4-2 and 4-3. Figure 4-4 shows the displacement contours on a horizontal section at 660 meters deep. Contours of displacement are all plotted from the time the shaft bottom had reached at the depth of 680 meters.

A number of displacement vectors, which show the size and the orientation of the shaft walls and bottom movements, are also plotted on Figures 4-2 and 4-3. The maximum displacement is about 1.6 mm and occurs at a shaft wall location that lies outside the close-up figure given. It has an orientation that coincides with that of a plane through σ_{Hmax}.

Figure 4-5 shows the deformation progress during the numerical excavation of Sector 7 (640 –680 meter deep). The deformation histories are plotted for chosen points on Diagonal 1 at a depth of 660 meters. These points lie on the shaft wall, 2.7 m, 5.4 m and 10.8 m away from the shaft wall respectively. The curves are plotted when the shaft had already been numerically excavated down to 680-meter under the condition that steady state had reached for each numerical blast round of 5 meter thickness.

Figure 4-6 shows the deformation build-up, picked up for four points spaced on the Diagonal 3 in the same way as for Diagonal 1. Note the generally lower magnitudes of deformation in this case, as the orientation of Diagonal 3 coincides with that of σ_{Hmin}.

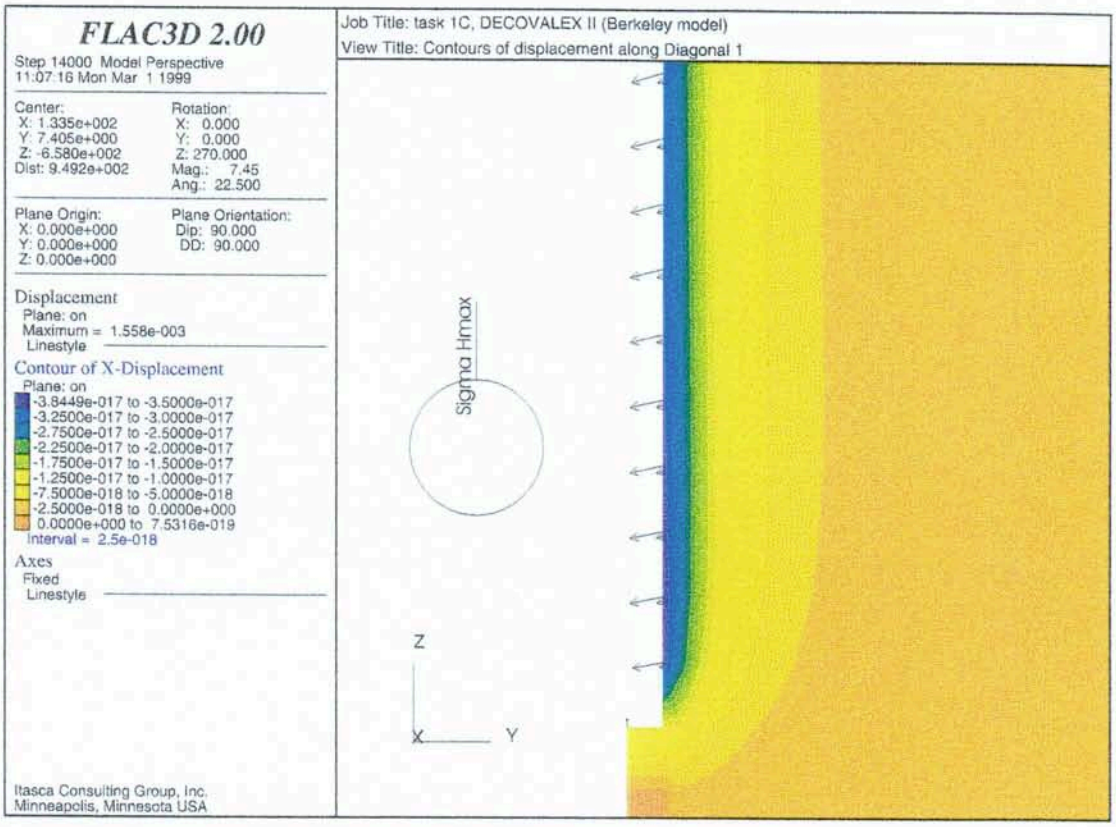

Figure 4-2 Contours of displacement plotted on a vertical plane along σ_{Hmax}. Arrows show the direction and the magnitude of displacements on the shaft wall.

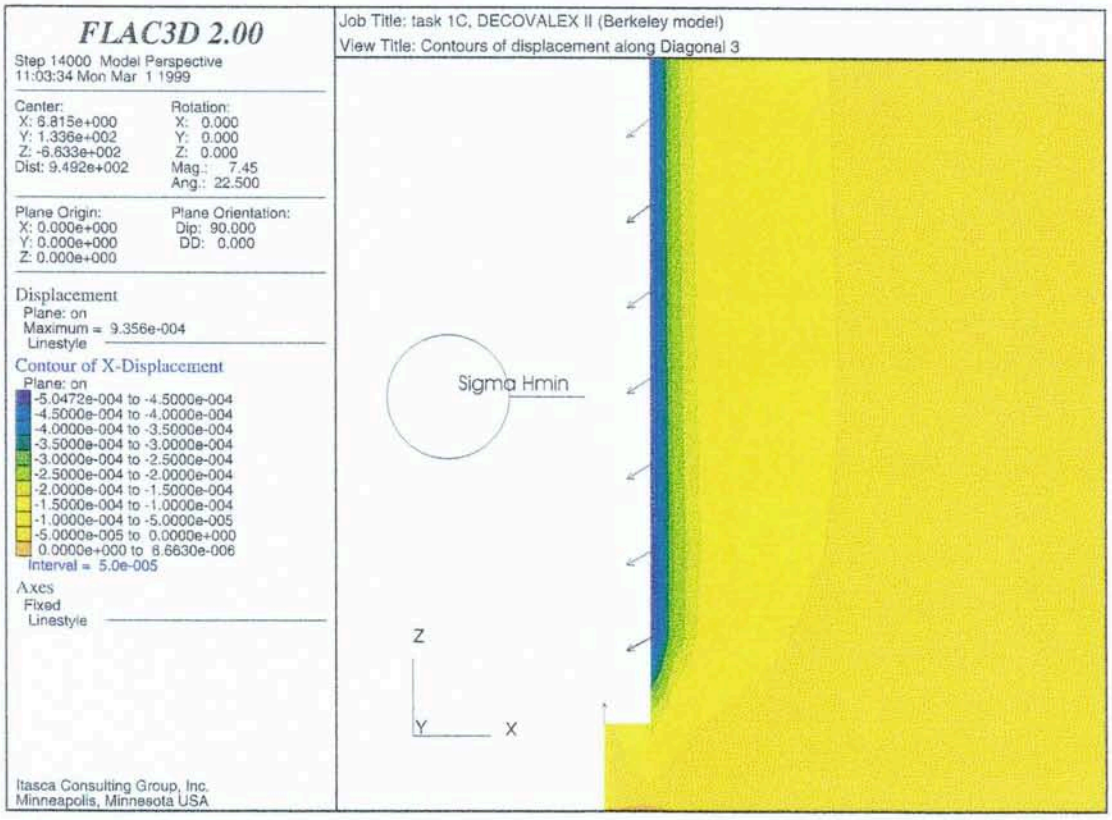

Figure 4-3 Contours of displacement on a vertical plane along the σ_{Hmin} axis. Arrows show the direction and the size of the displacements on the shaft wall.

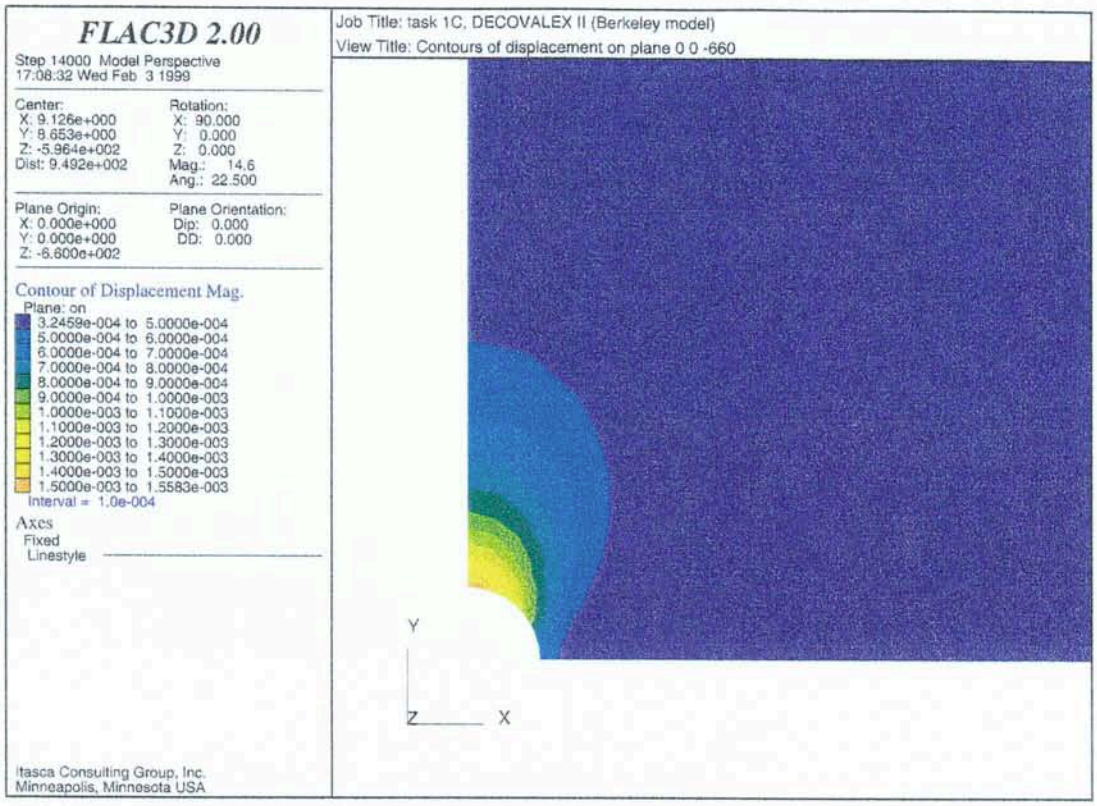

Figure 4-4 Contours of displacement on a horizontal plane at a depth of 660 meters.

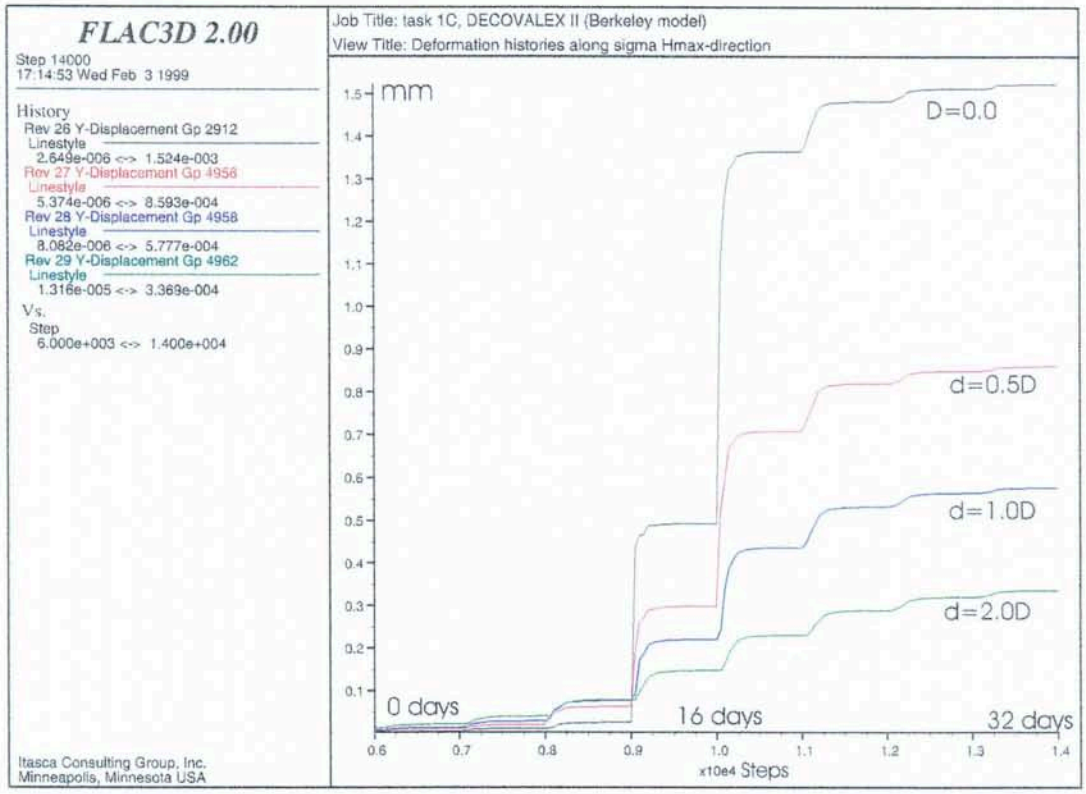

Figure 4-5 Deformation histories along Diagonal 1(σ_{Hmax} direction) at four points spaced at d=0.0, d=0.5D, d=1.0D and d=2.0D from the shaft wall. D denotes the diameter length of the shaft.

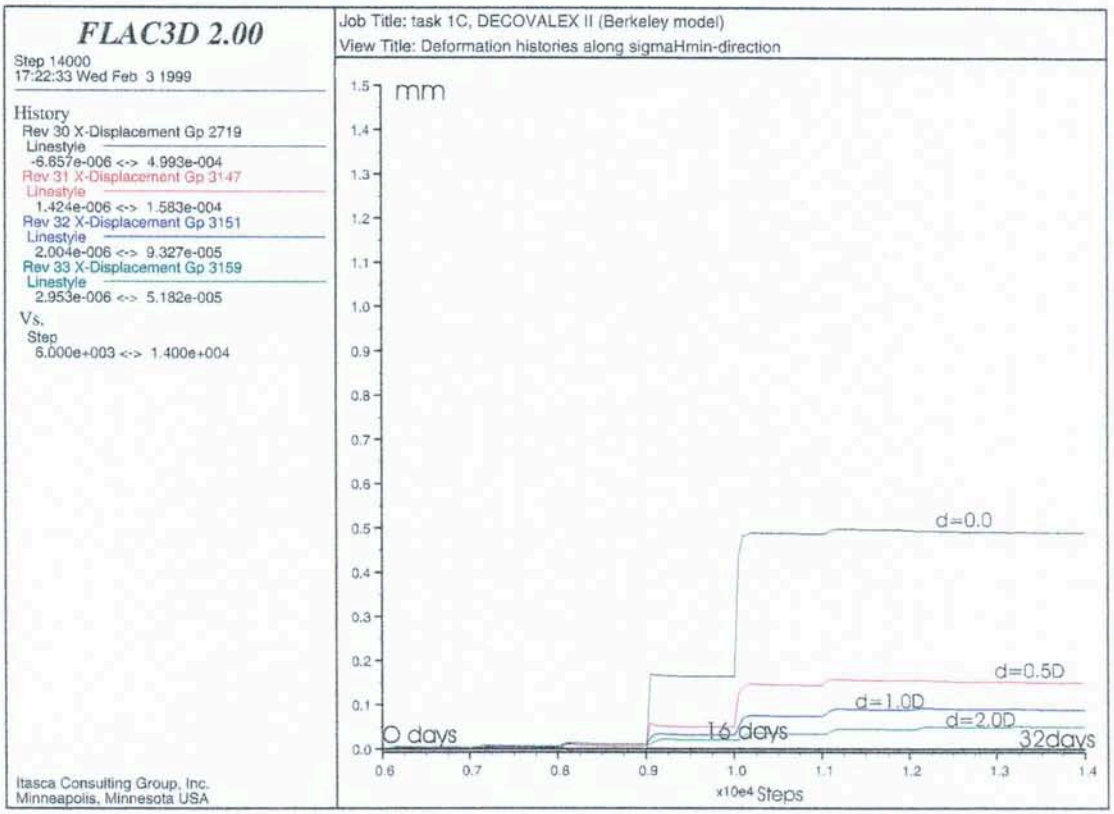

Figure 4-6 Deformation histories along Diagonal 3(σ_{Hmin} direction) at four points spaced distances from the shaft wall as given in caption of Figure 4-5.

Figure 4-7 shows the convergence of the shaft wall along Diagonal 1 and 3 at 660 meters of depth. Here again, the data were collected when Sector 7 had been fully excavated and the general steady state condition had been reached. Note that according to NIREX , the convergence along any diameter of the shaft is the sum of the inward displacement of the shaft walls at the two endpoints of that diameter.

Common in all deformation histories shown here are two "jumps", different in size, that correspond to the states where the shaft bottom has reached 660 and 665 meter of depth respectively. As the deformations are monitored at 660 meter deep, it is first at this level that the rock inside the shaft above this level is fully removed. At the depth of 665 meter, the shaft bottom has already passed the monitoring level by 5 meters and the deformations are most obvious.

The jumps in the deformation appear to have taken place under no or very little elapse of time (the near vertical portion of the jumps). This feature is indeed associated with the fact that the modelling procedure is such that the excavation of each numerical blast round is accomplished instantaneously.

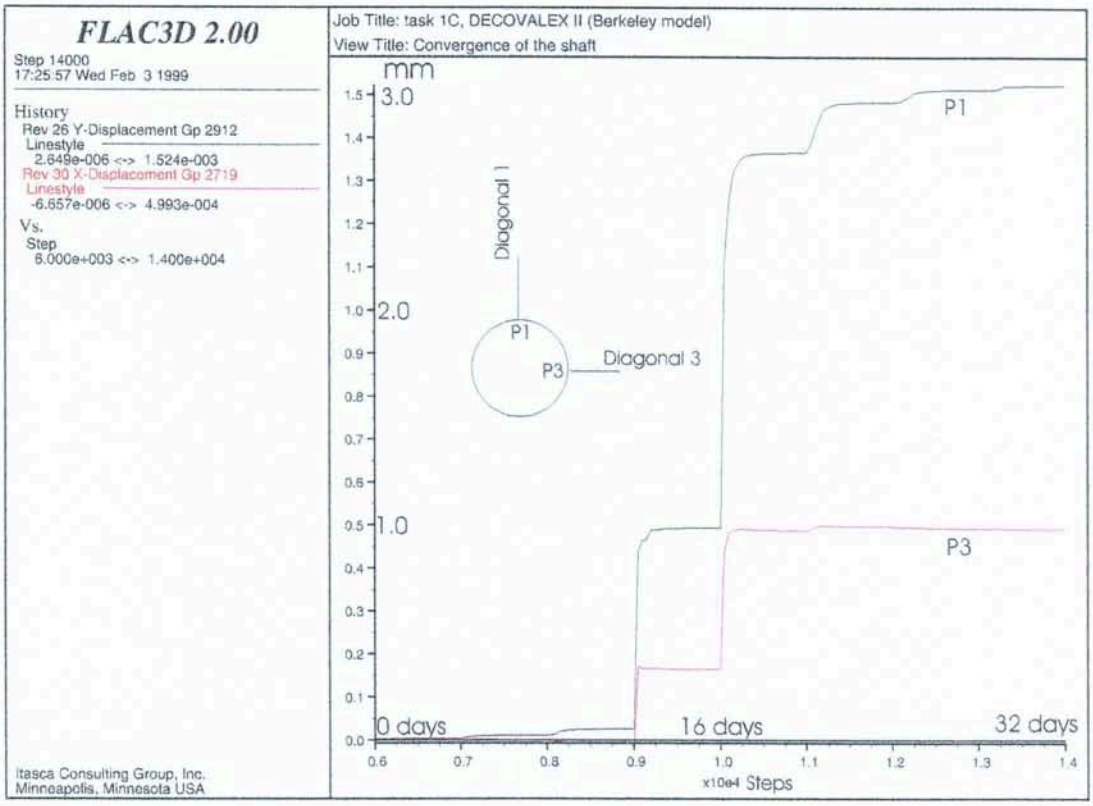

Figure 4-7 Convergence of the shaft at the two points shown.

Figure 4-8 shows the variation of the radial (σ_r) and the tangential stress (σ_t) during the excavation of Sector 7. The data are collected from a grid zone centroid closest to the nominal point P1 on the shaft wall. Here again the step-wise form of the curves illustrate the fact that the numerical excavation of each blast round was performed with no time elapsed. Figure 4-9 shows similar curves for a data collecting point closet to nominal point P3 on the shaft wall.

Figure 4-10 shows the distribution of the tangential and the radial stresses around the shaft at the depth of 660 meters. According to NIREX, the plots should include magnitudes of theses stresses at four nominal points on Diagonal 1 and Diagonal 3 respectively; the points being spaced on the shaft wall, 2.7 m, 5.4 m and 10.8 m from the shaft wall. In FLAC^{3D} the stresses associated with each grid zone are calculated at the centroid of that zone. Therefore the grid zones that their centroids lied closest to the nominal points produced the approximate tangential and radial stresses needed to include on the plots.

On the figure, the magnitudes of the in-situ stresses, σ_{Hmax} and σ_{Hmin} are also indicated with straight lines, in order that stress concentrations can readily be compared with the initial *in-situ* principal stresses.

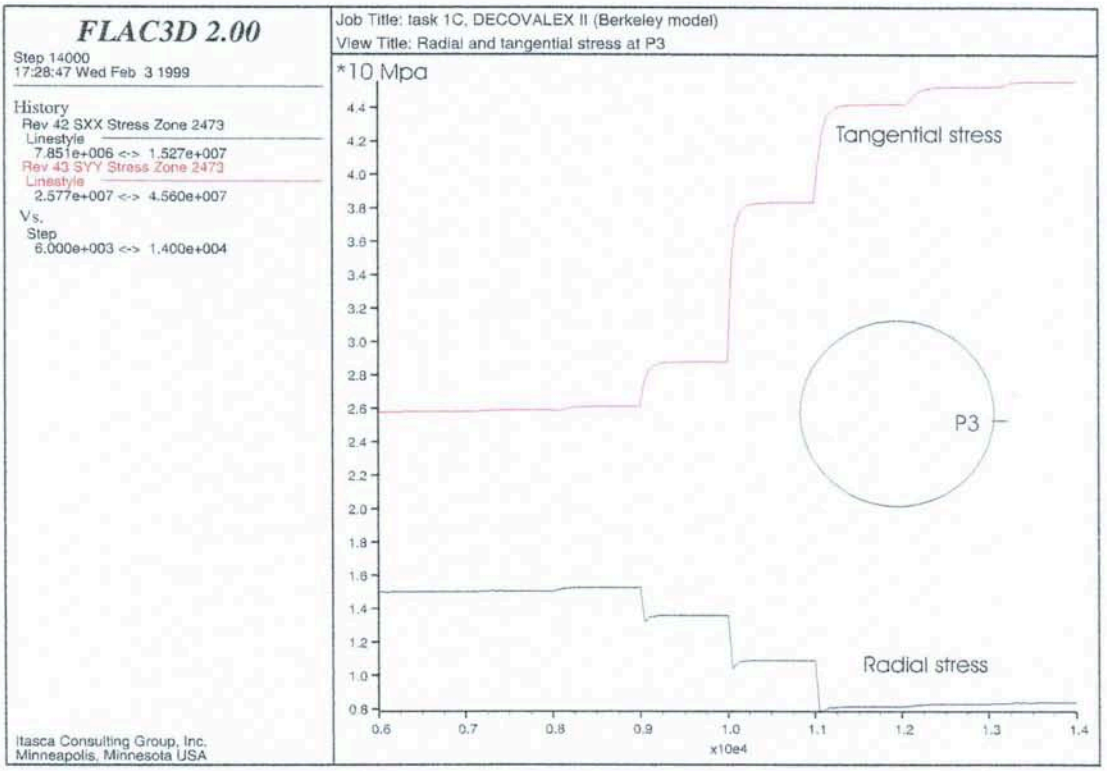

Figure 4-8 Radial and tangential stress at the nominal location P3. Data are collected from a depth of 660 m.

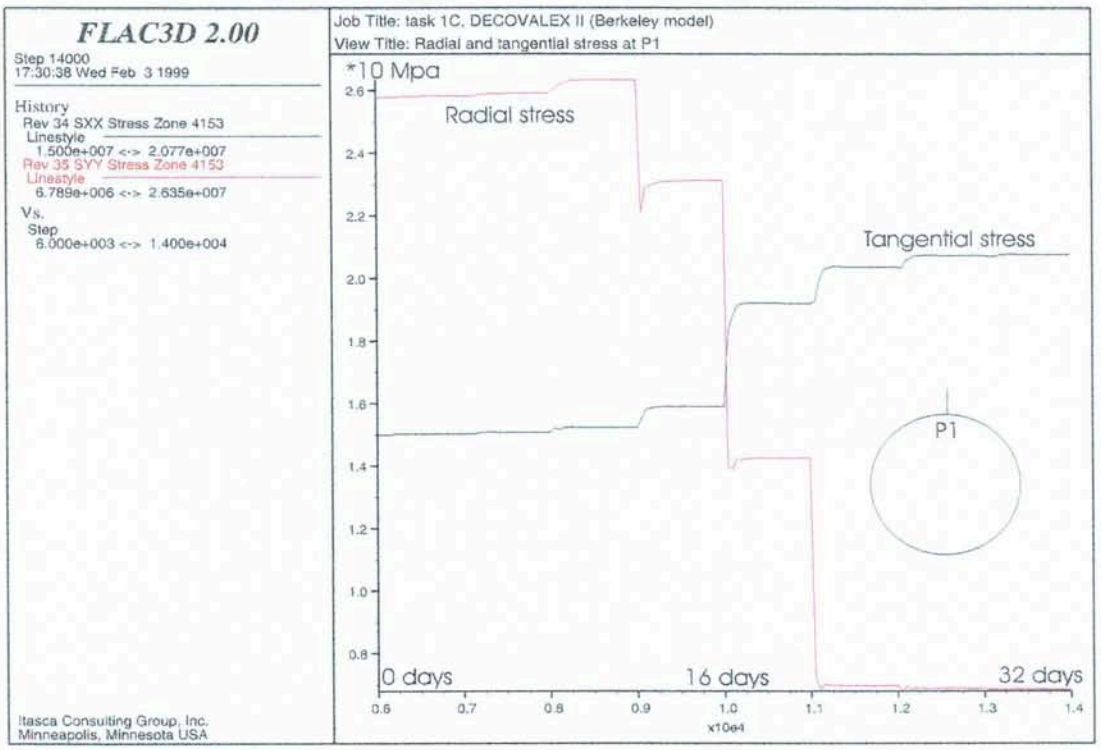

Figure 4-9 Radial and tangential stress at the nominal location P1. Data collected from a depth of 660 m.

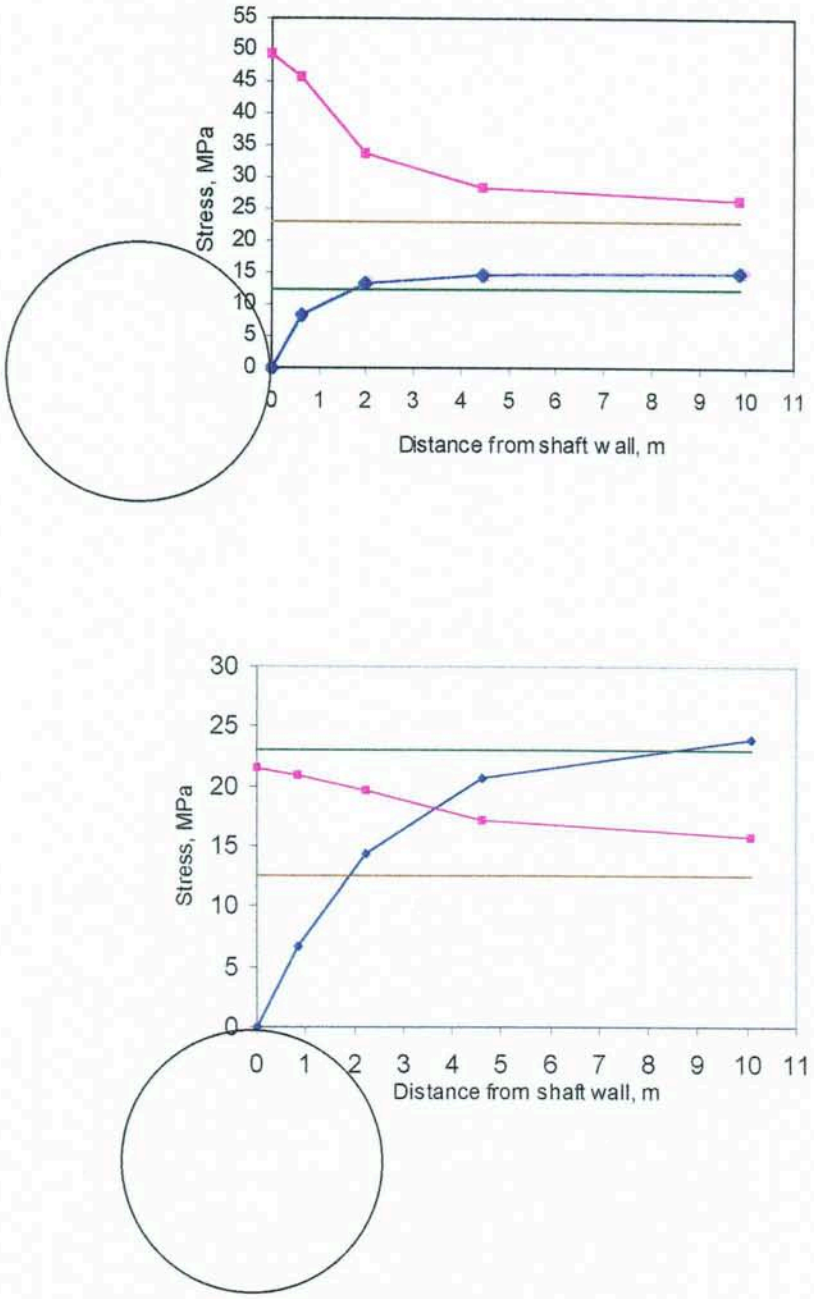

Figure 4-10 Distribution of radial and tangential stress as a function of distance from the shaft walls. Data are collected from a depth of 660 m.

Stress distribution shown on the figure are calculated when the shaft had reached the 680-meter level with steady state condition being fulfilled for each numerical blast rounds being removed.

As was expected, the largest concentration of the tangential stress, σ_t, occurs at the shaft wall on Diagonal 3, and its magnitude reaches as large as about two times the *in-situ* major principal stress, σ_{Hmax}.

Clearly, the disturbances of the *in-situ* stress field, as a result of the shaft sinking, extend beyond the distance of 10.8 meters (2 × shaft diameter) from the shaft wall. The disturbances presumably reach a distance of about 3 × shaft diameter (16.2m), beyond which the induced stress changes are insignificant.

In the context of the equivalent continuum material model used, the Excavtion Damage Zone would mean the detection of the grid zones in the immediate vicinity of the shaft, at which the failure criterion adopted is violated. Violation takes place when the stress components at a point are intensely increased or decreased such that they no longer remain in relationship to the strength of the rock at that point dictated by the failure criterion.

Under the conditions and assumptions described for the mechanical simulations, no failed grid zones were found out. The simulations could not, therefore, capture any Excavation Damage Zone

4.4 Hydrogeological computations

4.4.1 Boundary conditions

The basic assumption in order to set up the hydraulic boundary conditions was that the expanded model block (see section 4.1) had a large enough size such that the hydraulic regime near the boundaries would not be affected because of the shaft excavation. Accordingly, the initial pore pressure distribution on the vertical boundaries was kept constant at all depths during the numerical runs. The same condition applied to the top boundary, where a constant pressure corresponding to the pore pressure at that level was applied to the boundary.

Two conditions were considered for the bottom boundary:

- "Constant head", where a constant pore pressure was applied to the boundary, which kept the pore pressure unchanged at that level throughout the numerical runs.
- "No flow", where no hydraulic communication with the rock mass beyond that boundary was made possible throughout the numerical runs.

4.4.2 Hydrogeological properties of the rock mass

The relevant hydrogeological parameters needed for the simulations were extracted from the data provided by NIREX, through protocol for Task 1C. These parameters are given in Table 4-2 below.

Table 4-2 Hydrogeological properties of the rock mass.

Parameter	Magnitude
Hydraulic conductivity	1×10e-9 m/sec
Porosity	0.08%
Fluid density	1000 Kg/m^3
Fluid modulus	1×10e9

4.4.3 The sequence of computations

The sequence of computations was similar to that used for mechanical simulations. From the top of the model block at 425 meter depth to the beginning of Sector 7 at 640 meters the shaft was numerically excavated in two sections. The upper section reached 600 meter deep and the lower section began at that depth and ended at 640 meter depth. The choice of breaking the computations into two section at 600 meter depth was merely because of recommendations made by NIREX to collect the data from that point.

Sector 7 was then excavated in eight, 5-meter thick rounds as described for mechanical computations.

In agreement with what was described for mechanical computations, it would have been more appropriate if the stretches 425–600 and 600-640 meters were excavated in 5-meter intervals too. It is belived, however, that any influence from these stretches on the hydrogeological behaviour of the rock mass associated with the excavation of Sector 7 would be minimal.

4.4.4 Results

Figure 4-11 shows the distribution of the pore pressure as a result of the shaft excavation. The plot shows the contours of pore pressure that correspond to the situation where the shaft front lied at 680 m depth.

It is to be mentioned that a common procedure in such numerical simulation is that the pore pressure is lowered to zero "instantaneously" for each section excavated. This is undoubtedly an over-simplification that otherwise may call for sophisticated procedures in order to compensate the possible influence of such routine on the results.

Figure 4-12 shows the pressure drawdown within boreholes RCM1 and RCM2 as a result of shaft sinking through Sector 7. Data are collected from 640 and 680 meter levels under the steady state condition at the base of Sector 7. Data collection began as soon as the shaft front passed the depth of 600 meters.

Although the pressure drawdown associated with the excavation of Sector 7 is controlled by sequential excavation of that sector, yet the overall pressure drawdown at the boreholes named appears to be very gradual. This is because the two bore holes are located outside the zone around the shaft, where the pore pressure drop is intensive. This can be seen on Figure 4-11.

Figure 4-13 shows the water inflow into Window 1 of Sector 7. Window 1 refers to the first half of Sector 7, which is located between 640 to 660 meter depth.

As shown on the figure, during the excavation of Window 1, the inflow into the walls of the shaft at this section increases stepwise with each round being excavated. The total inflow from the walls of Window 1 was approximately 2.1 lit/min.

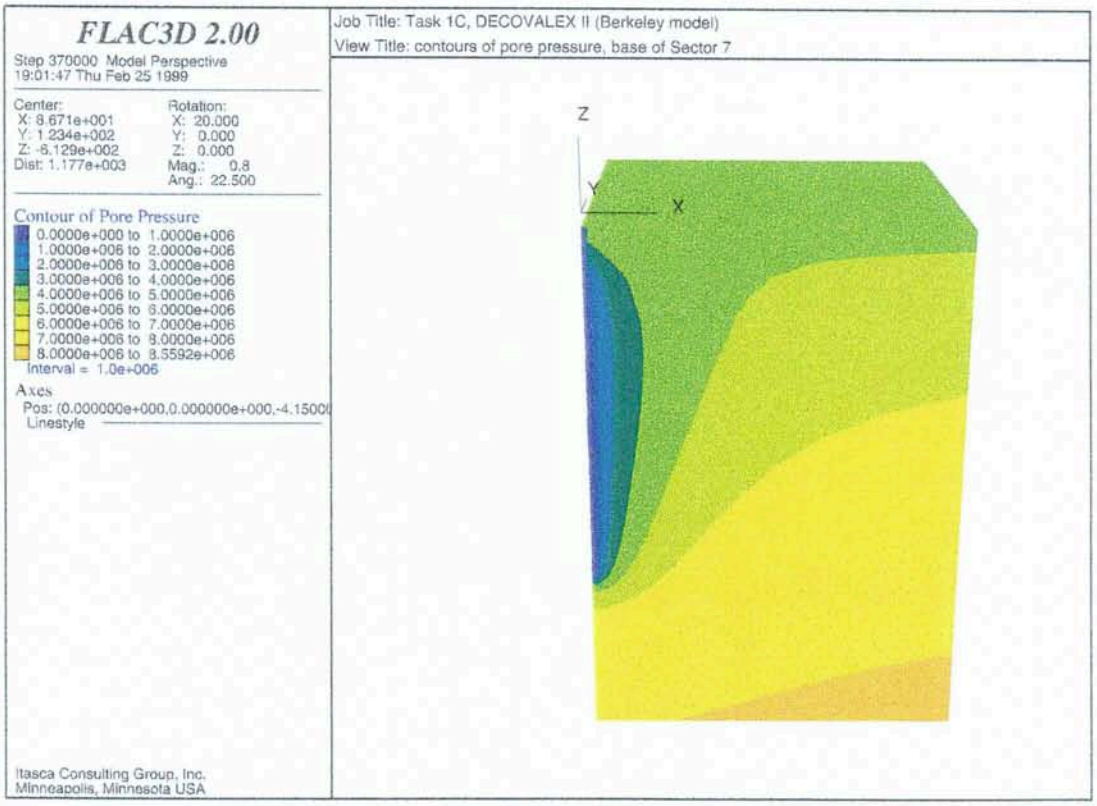

Figure 4-11 Contours of pore pressure resulting from the full excavation of sector 7.

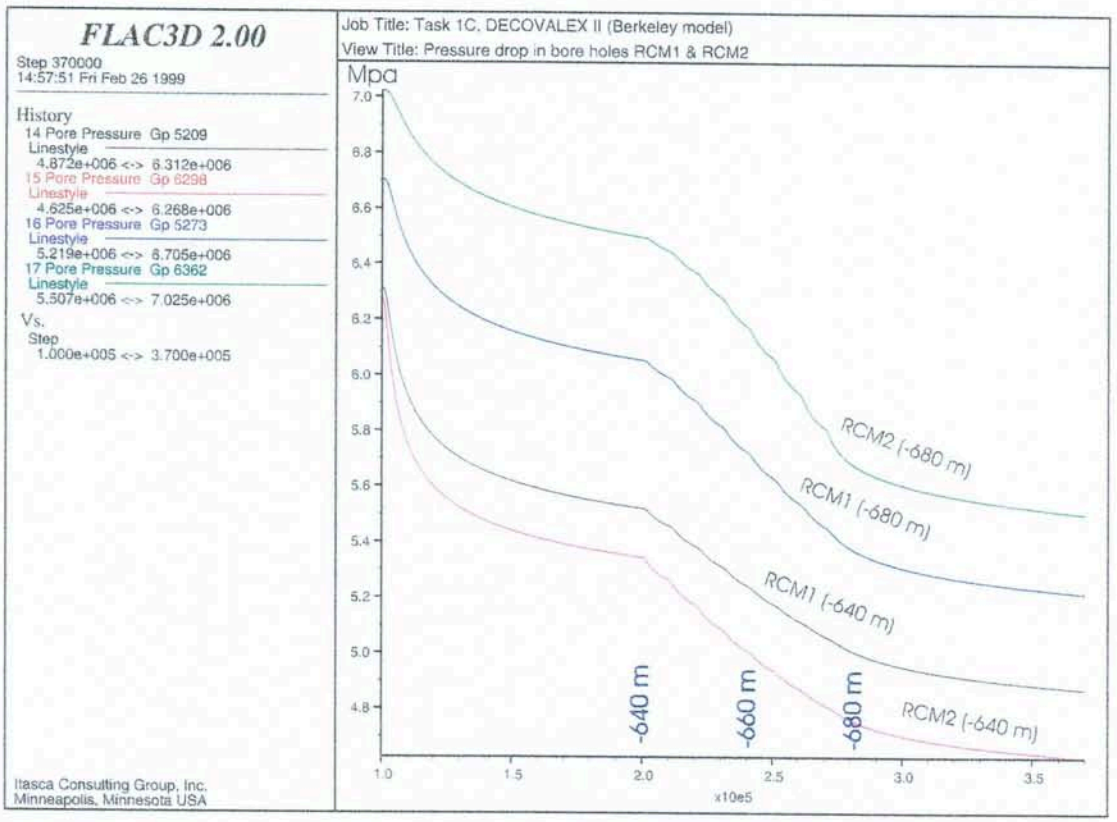

Figure 4-12 Pressure drawdown in boreholes RCM1 and RCM2 resuting fromshaft sinking through Sector 7. Data are collected at the depths of 640 and 680.

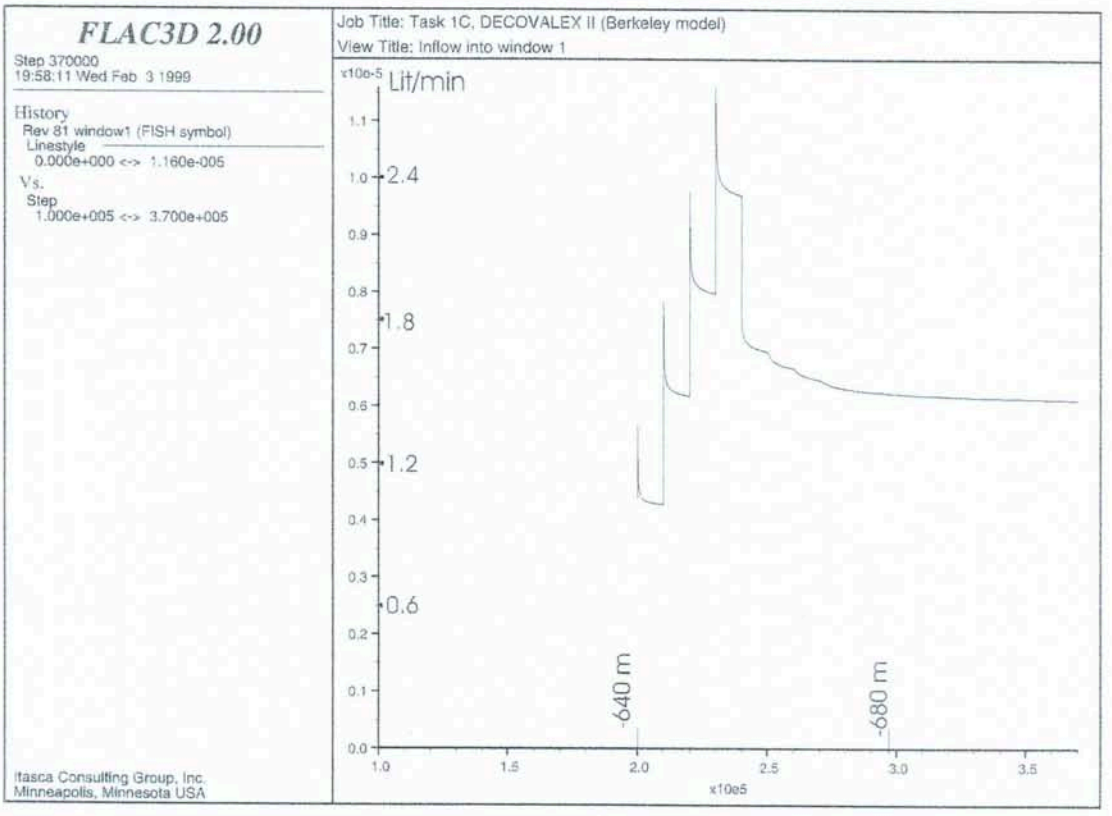

Figure 4-13 Inflow into Window 1 during the excavation of Sector 7 in full.

As the excavation of the shaft proceeds, the inflow into Window 1 diminishes gradually until it stabilises at about 1.65 lit/min when the shaft has already reached 680 meter deep. This is shown on the second part of the plot that begins at point A (marked on the plot).

Fig 4-14 shows the inflow into Window 2. Note the decrease of the inflow when the last 5-meter of Window 2 was removed. This reflects the effect of the hydraulic boundary condition at the bottom of the model block, where no communication of flow with the outside was possible at the bottom; i.e. no water was allowed to seep into the model block from the bottom side in order to partly compensate the water lost into the shaft.

The hydrogeological computations were repeated with a constant head at the lower boundary, where communication of flow with the outside was possible. Flow into Window 1 took place in an identical manner as for the previous case with no flow at the lower boundary, see figure 4-13. Flow into Window 2, however, took place differently. Removal of the last 5 meters of the window led to the increase of the flow, see Figure 4-15. Clearly the maintained turnover of the water inside the model block enabled the inflow into the window to increase at all times.

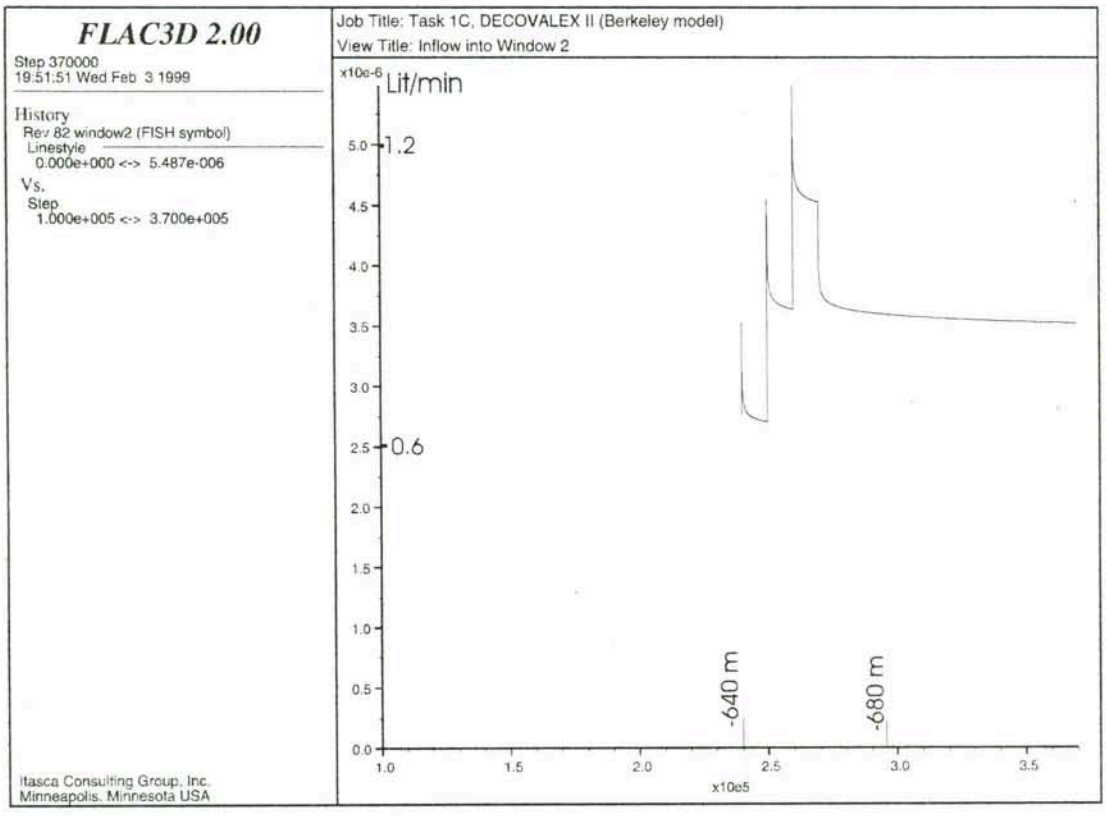

Figure 4-14 Inflow into Window 2. "No flow" Hydraulic boundary defined the lower boundary of the model block.

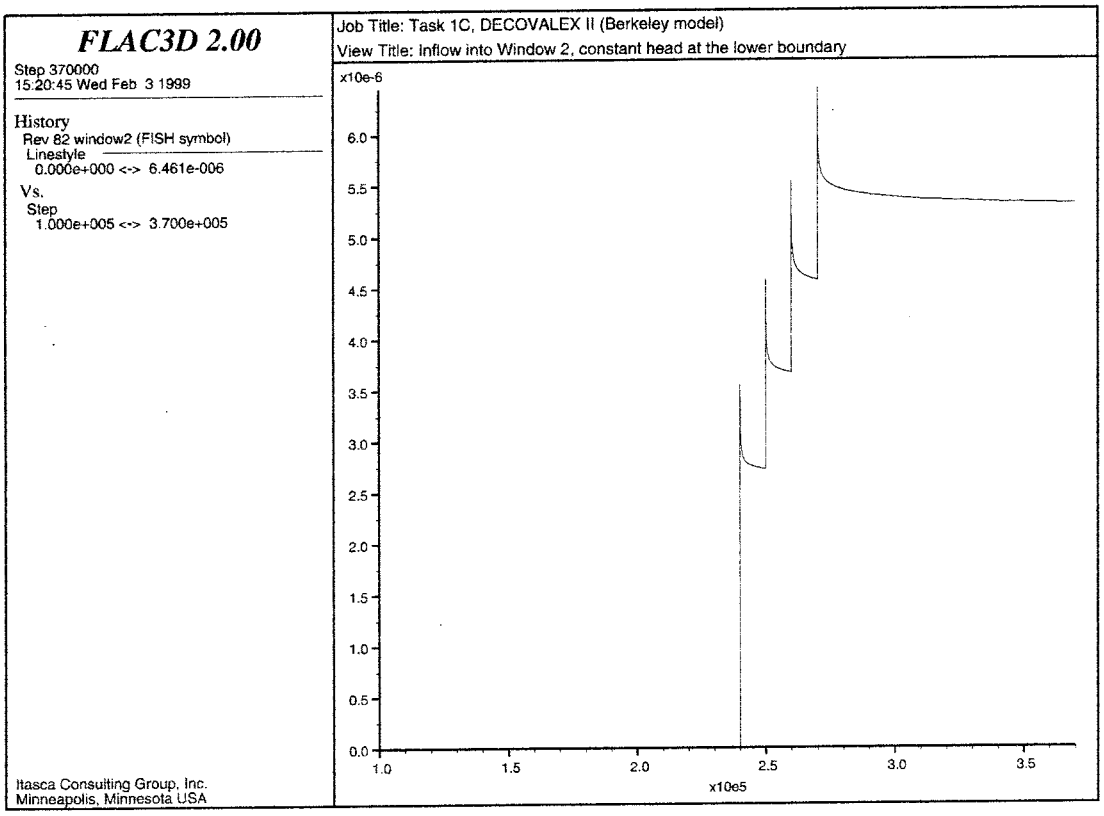

Figure 4-15 Inflow into Window 2, where a "constant head" hydraulic boundary defined the lower boundary of the model block.

5 The Avignon model

5.1 Preface

Simulations carried out so far may be regarded as being elements in a first approach . They provided insight into the most common consequences, a shaft sinking of such dimensions would bring about in a hard rock environment. It is, nevertheless, possible to improve the simulations by introducing explicit features in the context of continuum formulations, such as zones with enhanced flow, which may bring the analyses closer to the field measurements and observations.

Within the framework for the Berkeley model, It was noticed that the mechanical disturbances caused by the shaft sinking were not of such intensities to produce any Excavation Damage Zone. This is obviously a numerical shortcoming that depends on the input parameters and the disability of the failure criterion used to capture the EDZ.

By adopting a new failure criterion, hereafter, it has been possible to capture the EDZ although with some limitations.

5.2 The grid

Having concluded that the overall size of the model block used in the previous simulations might not have been large enough for hydrogeological computations and also in order to harmonise further the model block size with those used by other research groups (see Lanru et al. 1998), a larger model block was built up.

The idea to include three major fault zones in the grid, necessitated a full size model block for hydraulic computations. No planes of symmetry could, therefore, be used. Clearly the number of grid zones in comparison to that of the Berkeley model increased by many folds.

As it was clear from the mechanical simulations of the Berkeley Model, the size of a grid for such simulations could be much smaller on a horizontal cross section, compared with that needed for the hydrogeological simulations. The new grid was, therefore , built in such a way that the "core" of grid (a right-angled parallelepiped with a side length of 80 meters) could handle the mechanical computations whereas the model block as a whole could cope with the hydrogeological computations.

Figure 5-1 shows a general view of the grid. A close-up top view of the grid is also shown in Figure 5-2. Note that the Two sub-grids, the core and the bulk of the model block, have different grid zone sizes; the side length of the cubic grid zone from the

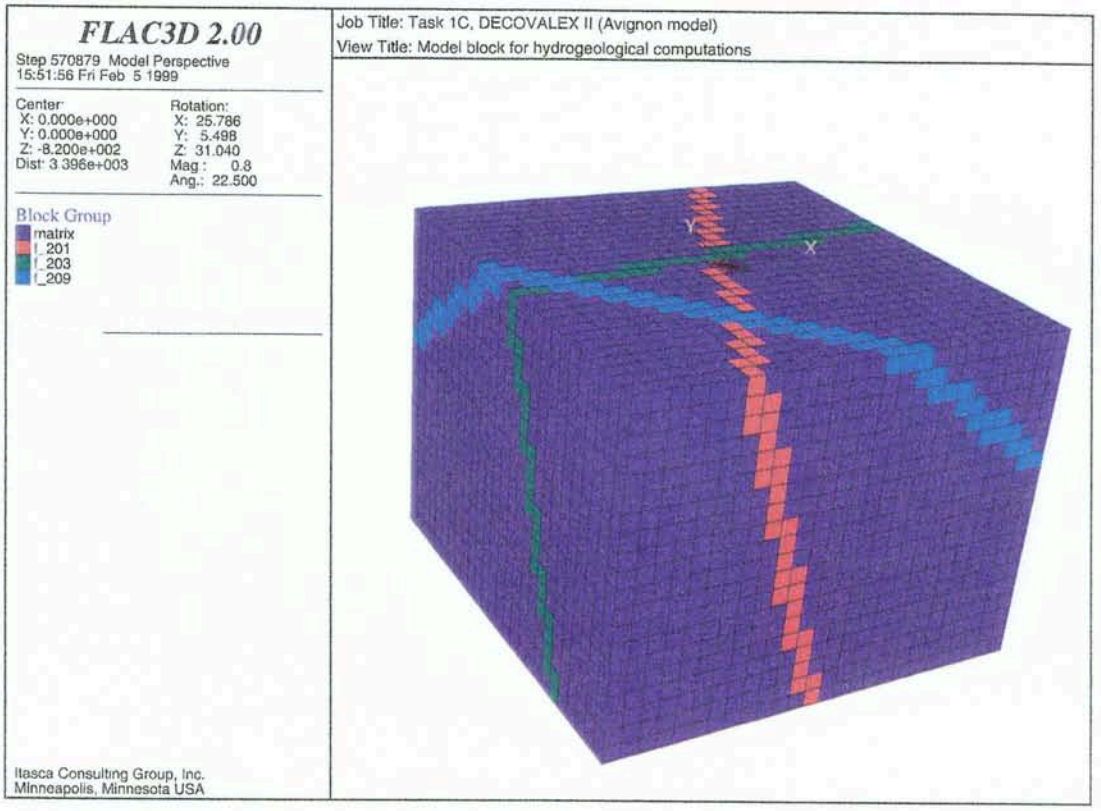

Figure 5-1 General view of the model block for hydrogeological computations.

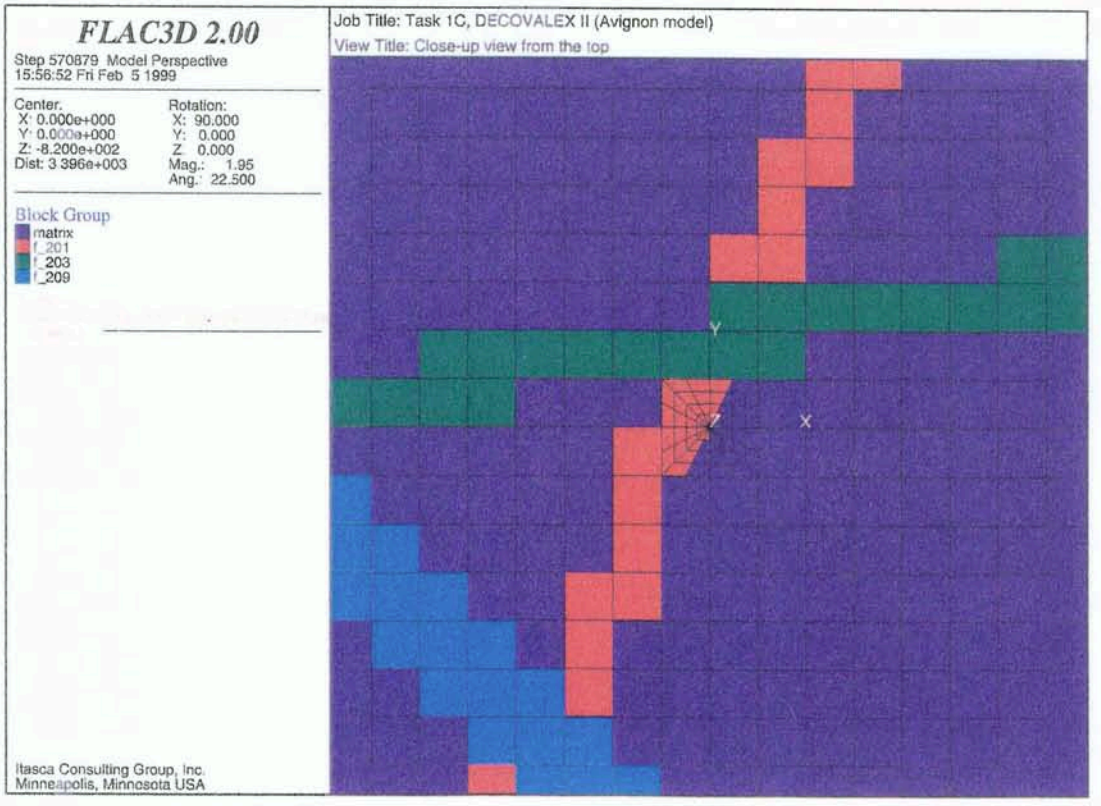

Figure 5-2 Close-up view (from the top) of the model block. Note the way the core is "attached" to the bulk of the model.

bulk is two times the base of the neighbouring grid zones belonging to the core at the interface.

FLAC^{3D}, Version 2.0 allows the user to attach faces of sub-grids together rigidly to form a single grid if certain conditions are met. The faces of the two sub-grids that are to be attached must be co-planar and lie within a relative tolerance of 10^{-6}. Also, dividing the side length of the larger grid zone from one side of the interface by the side length of the smaller grid zone from the other side must render an integer.

The core of the grid that contained the shaft was discretized very finely. The thickness of the grid zones in the immediate vicinity of the shaft was not larger than about 0.65 meter. This fine discretizaton was necessary in order to be able to study the excavation damage zone. The sub-grid used for mechanical computations needed only be one fourth of the complete core. The flow zones played no role in these computations and use of symmetry planes were, therefore, possible. Fig 5-3 shows a close-up view of the sub-grid used for the mechanical computations. It contained about 26000 grid zones

As could be seen, the bulk of the model block is discretized in such a way to produce grid zones that are solely cubes of the same size. In this way it was possible to model the selected fault zones that cut through the rock mass in a more statistically homogeneous manner. The bulk had about 20000 grid zones.

The modelled fault zones were active in hydrogeological simulations. They were intended to merely act as features with enhanced hydrogeological properties within a matrix having much lower such properties. The fault zones may thus be called "flow zones" in this report to underline the fact that they were mechanically inactive. Figure 5-4 shows a half of the model block; the front half of the model being removed; illustrating the flow zones and the shaft.

Each flow zone, having an orientation (dip and azimuth) that was an estimate of the corresponding natural fault zone, consisted of a number of grid zones that lied within a thickness of 25 meters. The flow zones, f 201, f 202, f 209, named after their true fault zones *in-situ*, contained 1601, 1565 and 1493 grid zones respectively.The flow zones together constitute 23% of the number of grid zones in the bulk.

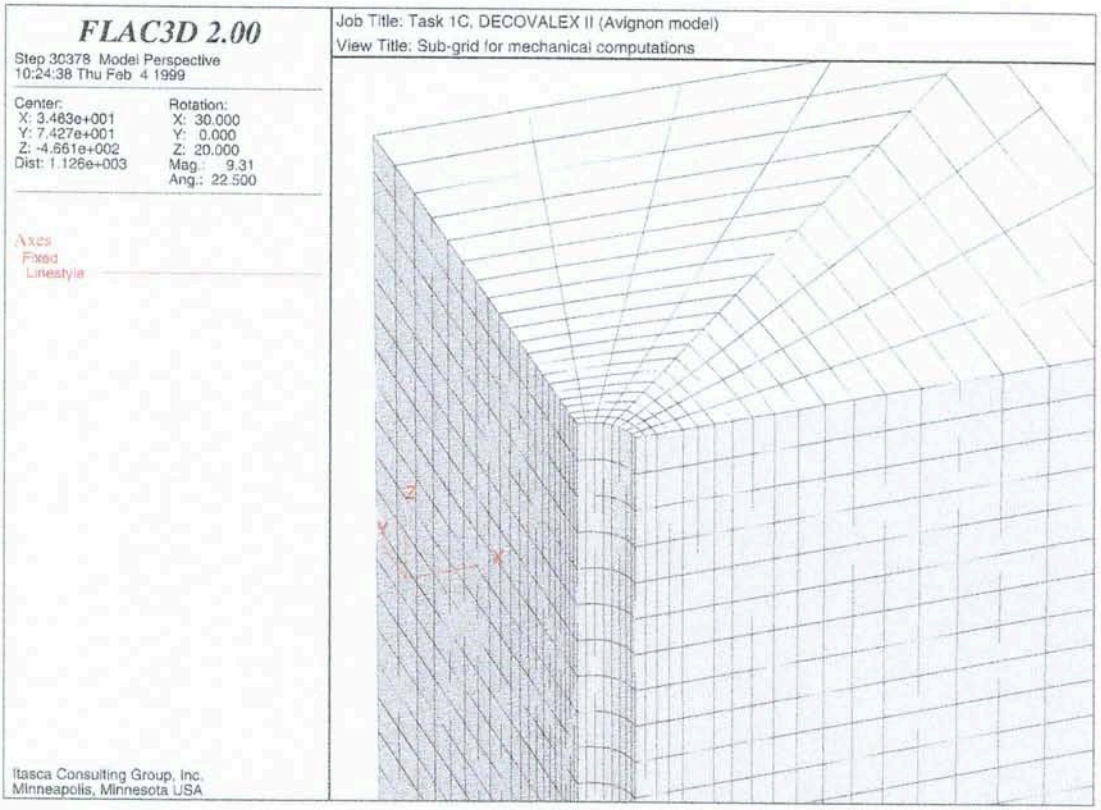

Figure 5-3 Close-up view of the sub-grid used for mechanical computations.

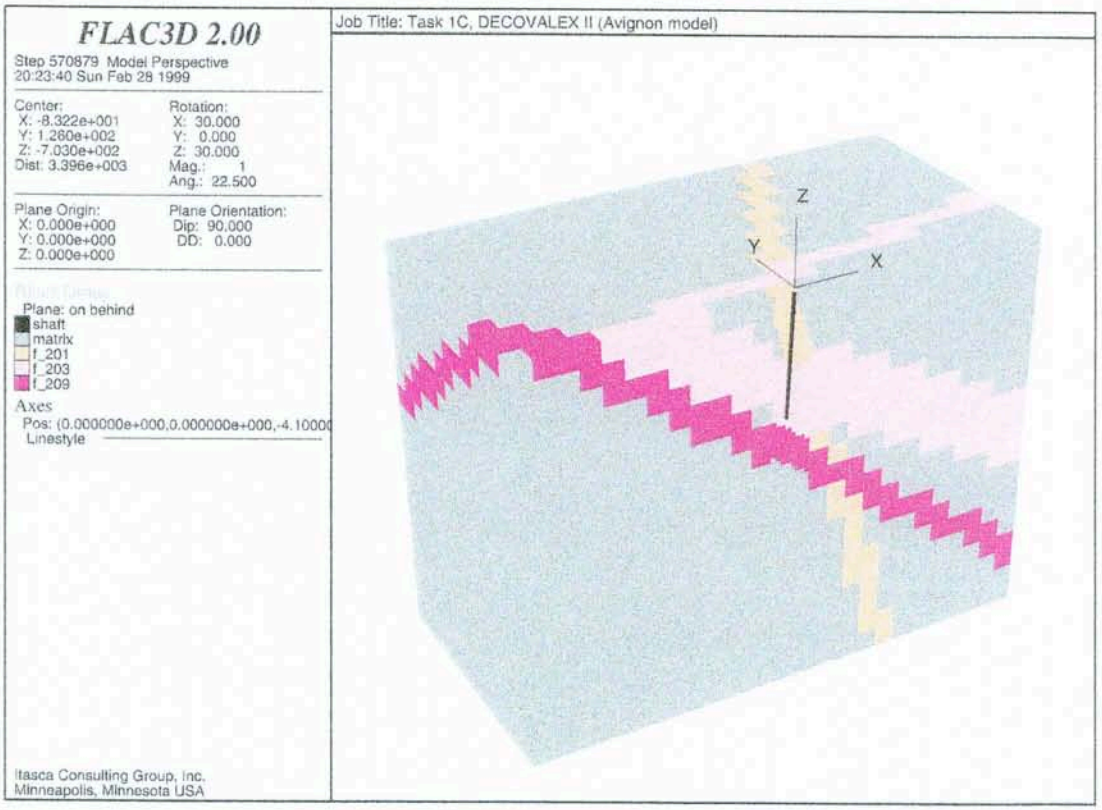

Figure 5-4 The rear half of the model block showing the flow zones and the shaft. The front half of the block is removed to expose the inside of the block.

5.3 Mechanical computations

5.3.1 Boundary conditions

As was mentioned earlier, the grid used for mechanical computations formed the core of the main model block. It was square on a horizontal section with a side length of 80 meters; the mechanical disturbances would not reach more than 3-4 times the shaft diameter. Boundaries were defined as for the Berkeley model, see section 4.3.1.

5.3.2 Failure Criterion

It is well understood that the excavation of an underground opening results in a damage zone in the rock mass within the intimate approximity of the opening. In many numerical modelling of underground openings; as noted in the Berkeley Model too; the damage zone is not captured by the simulations, in particular in works where the rock is modelled as a continuum. Presumably the failure criteria chosen to control the failure in rock , generally fed with high strength values as in-put parameters in the first place, turn out to be incapable of revealing the damage zone.

Mohr-Coulomb failure criterion has been used vastly to describe the brittle failure of rock. Hoek and Brown failure criterion has also been used extensively in recent years in studying the brittle failure of rock. These criteria are, however, incapable of capturing the onset of brittle failure perfectly, nor to estimate the minimum depth to which the brittle failure propagates (see e.g. Grimstad and Bhasin, 1997)

Martin has recently showed that (Martin, 1997) the maximum depth of stress-induced brittle fracturing around a circular test tunnel in massive granite could be approximated by a criterion that only considered the cohesive strength of the rock mass. It was postulated that around underground openings, the brittle failure process is dominated by a loss of the intrinsic cohesion of the rock mass such that the frictional strength component can be ignored.

In 1980, Hoek and Brown (Hoek and Brown, 1998) proposed an empirical failure criterion that is now widely used in rock engineering and is usually expressed in the following form:

$$\sigma_1 = \sigma_3 + \sqrt{m\,\sigma_c\,\sigma_3 + s\,\sigma_c^{\,2}} \qquad 5\text{-}1$$

where

σ_1 and σ_3 are the major and the minor principal stresses at failure

σ_c is the uniaxial compressive strength of the intact rock and

the empirical constants, m and s are related in a general sense to the angle of internal friction φ, and the rock mass cohesive strength C.

For both the Mohr-Coulomb or the Hoek&Brown failure criteria, it is implicitly assumed that the cohesive (C or s) and the frictional (φ or m) strength component are mobilized simultaneously.

For the boundary of a tunnel, where $\sigma_3 = 0$, Equation 5-1 reduces to:

$$\sigma_1 = \sqrt{s}\,\sigma_c^{\,2} \qquad 5\text{-}2$$

Martin showed, based on microseismic evidence, that a constant deviatoric stress as given in the form:

$$\sigma_1 - \sigma_3 = 1/3\,\sigma_c \qquad 5\text{-}3$$

could express the state of stress corresponding to the damage-initiation close to a circular tunnel in hard rock. Other researchers have also found that the initiation of fracturing in uniaxial laboratory tests occurs between 0.25 and 0.5 σ_c for a wide variety of rock types.

The constant deviatoric stress equation can be combined with the Hoek&Brown failure criterion to arrive at:

$$\sigma_1 = \sigma_3 + \sqrt{s}\,\sigma_c^{\,2} \qquad 5\text{-}4$$

by setting the frictional constant m to zero in order to reflect that the frictional strength component has not mobilized. The above equation render the value of s as:

$s = 0.112$

It has been shown that (Hoek, 1990) the angle of rock friction and the cohesion may be derived from the Hoek&Brown failure criterion as follows:

$$\varphi = 2\tan^{-1}\sqrt{N_\varphi} - 90 \qquad 5\text{-}5$$

$$C = \sigma_c^{\,M} / 2\sqrt{N_\varphi} \qquad 5\text{-}6$$

Where

$$N_\varphi = (1+\sin\varphi) / (1-\sin\varphi) \qquad 5\text{-}7$$

and

$$\sigma_c^{\,M} = \sigma_3 (1 - N_\varphi) + \sqrt{m\,\sigma_c\,\sigma_3 + s\,\sigma_c^{\,2}} \qquad 5\text{-}8$$

For the onset of failure; the state during which friction is not mobilized ($\varphi = 0$); the above equation reduces to:

$$\sigma_c{}^M = \sqrt{s}\,\sigma_c{}^2 = 0.33\,\sigma_c \qquad 5\text{-}9$$

and Equation 5-6 reduces to

$$C = \sigma_c{}^M / 2 \qquad 5\text{-}10$$

Consequently

$$C = 0.33\sigma_c / 2 = 0.165\,\sigma_c \qquad 5\text{-}11$$

The failure criterion outlined was used in the mechanical computations in order to estimate the excavation Damage Zone.

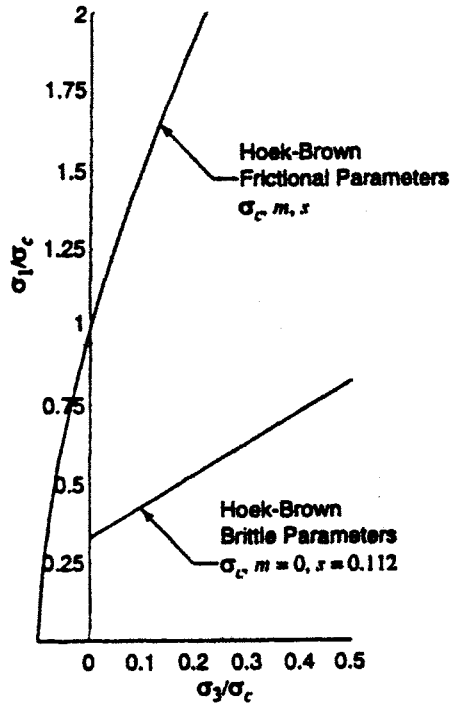

Figure 5-5 Illustration of the Hoek&Brown envelope for friction (sc, m, s) and brittle (sc m 0.0, s = 0.112) parameters.

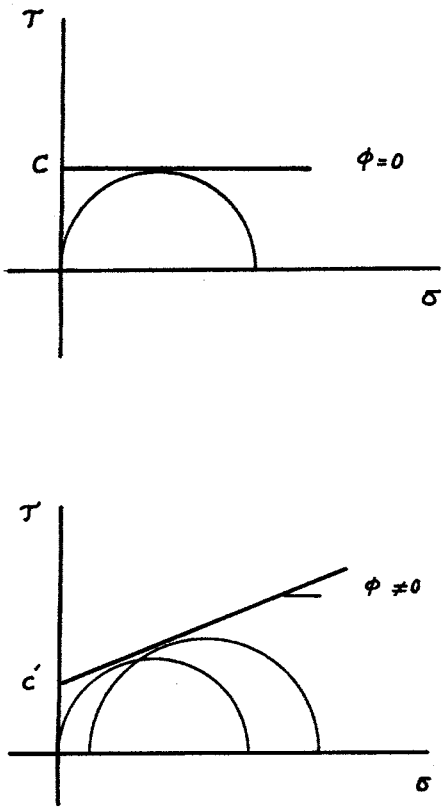

Figure 5-6 Martin's criterion for the onset of brittle failure in terms of (a) Mohr-Coulomb parameters and (b) a normal Mohr-Coulomb criterion.

5.3.3 Mechanical properties

NIREX had submitted the modulus of deformation for the rock mass as 65 GPa, which was used in the Berkeley model. The value had been estimated to represent the overall modulus of deformation for the rock mass. A look through some literature that dealt with the modelling of similar rock masses, studying the deformation magnitudes that were obtained for the Berkeley model and discussions with other research groups working on Task 1C, led to re-estimating the modulus by resorting to the other data available from the site investigations and the laboratory tests, see section 3.2.

It has been shown (Stille *et al*, 1982) that the relationship between the Rock Mass Rating, RMR (Bienawski, 1976) and the equivalent modulus of elasticity for a rock mass may be approximated by Equation 5.3.1 as follows:

$$Em = 2\,RMR - 100 \qquad 5\text{-}12$$

Where Em is the equivalent modulus of elasticity of the rock mass.

NIREX submits the value of 71.79 for RMR. Considering this value of RMR, Equation 5-12 renders an approximate value of 44 MPa for Em. Other research groups reported in the meeting at Avignon that they had arrived at similar or even smaller values of Em in

their later assessments of the input data. The value of 44 MPa, was accordingly used in the simulations that are reported in the remaining part of this report. Table 5-1 lists the parameters used for mechanical computations.

Table 5-1 Parameters used in the mechanical computations

Parameter	Magnitude
Interpreted E_{mass}	44 GPa
Poisson ratio	0.24
Angle of internal friction	0.0
Cohesion	26.2 MPa
Tensile strength$_{(mass)}$	0.0

5.3.4 The sequence of computations

5.3.5 Results

Figure 5-7 shows the contours of displacement in the direction of σ_{Hmax} (Diagonal 1). The maximum size of the displacement is 2.3 mm and refers to a point on the shaft wall that is not shown on close-up figure shown. Figure 5-8 shows the displacement contours along σ_{Hmin}.(Diagonal 3) The contours are plotted after the shaft had reached 680 m depth and the overall steady state condition was fulfilled.

Figure 5-9 shows the deformation progress during the numerical excavation of Sector 7 (640 –680 meter deep). The deformation histories are plotted for four chosen points on Diagonal 1 at a depth of 660 meter. These points lie on the shaft wall, 2.7 m, 5.4 m and 10.8 m away from the shaft wall respectively. The curves are plotted when the shaft had already been numerically excavated down to 680-meter under the condition that equilibrium had reached for each numerical blast round of 5 m thickness being removed.

Figure 5-10 shows the deformation build-up, collected for four points spaced on the Diagonal 3 in the same way as for Diagonal 1. Note the generally lower magnitudes of deformation in this case, as the orientation of Diagonal 3 coincides with that of σ_{Hmin}.

Figure 5-11 shows the convergence of the shaft wall along Diagonal 1 at the depth of 660 meters. The data are collected when the excavation reached the bottom of sector 7 under the general steady state condition. The contours of displacement along Diagonal 1 plotted on a horizontal section at 660 m depth has also been shown on the figure. Note

that according to NIREX, the convergence along any diameter of the shaft is the sum of the inward displacement of the shaft walls at the two endpoints of that diameter.

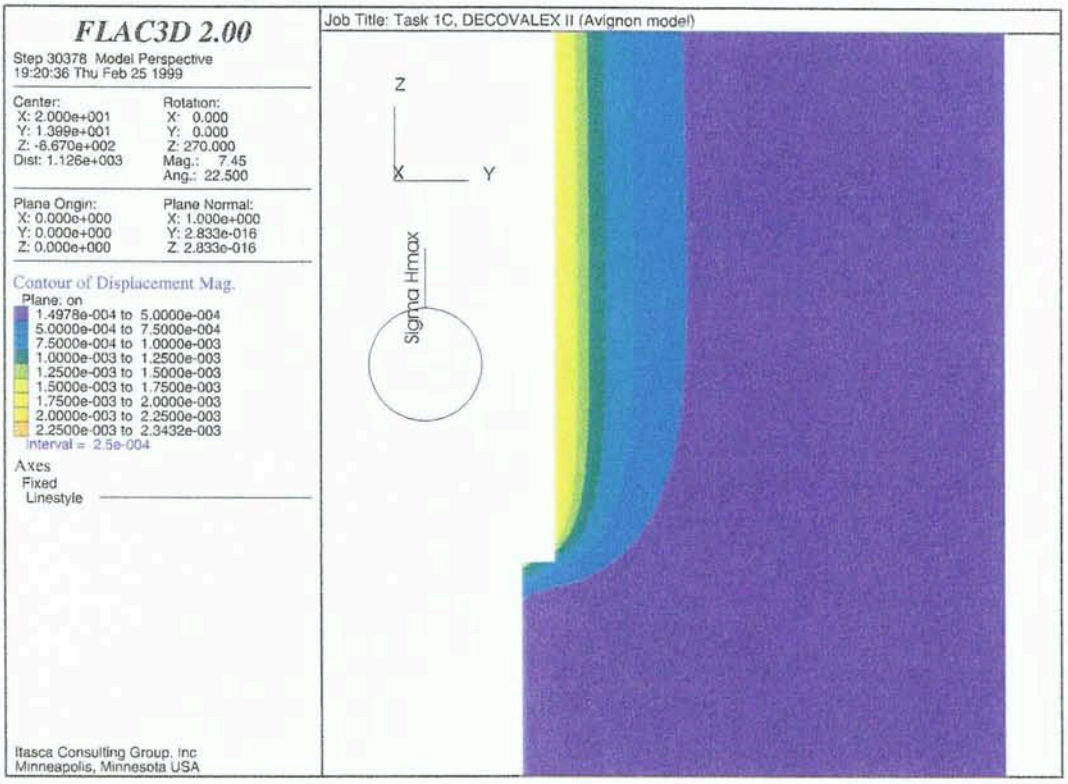

Figure 5-7 Contours of displacement on a vertical plane along σ_{Hmax} direction

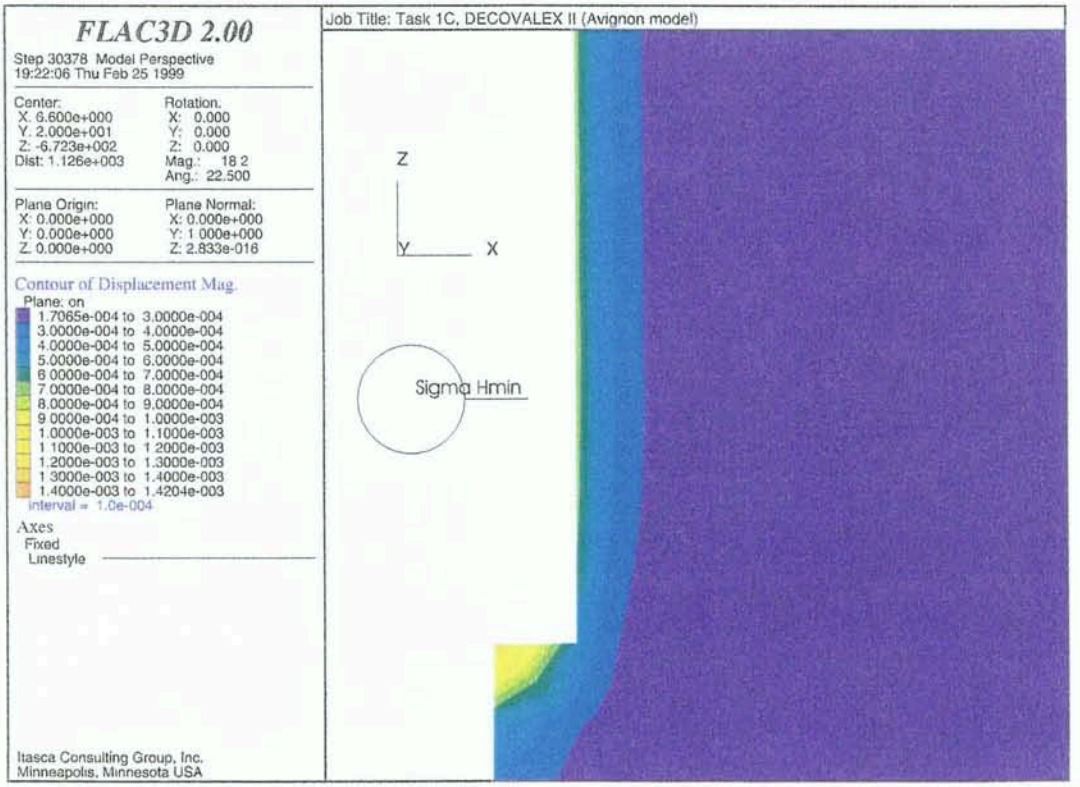

Figure 5-8 Contours of displacement on a vertical plane along σ_{Hmin} direction.

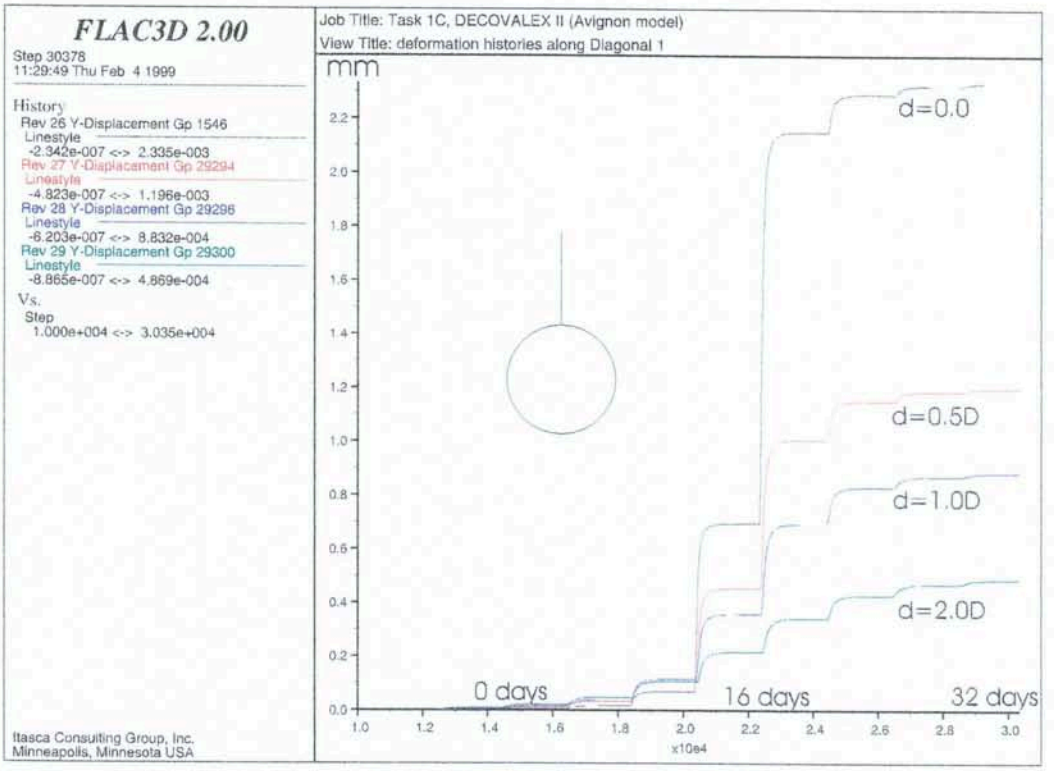

Figure 5-9 Deformation histories along Diagonal 1(σ_{Hmax} direction) at four points spaced at d=0.0, d=0.5D, d=1.0D and d=2.0D from the shaft wall. D denotes the diameter length of the shaft.

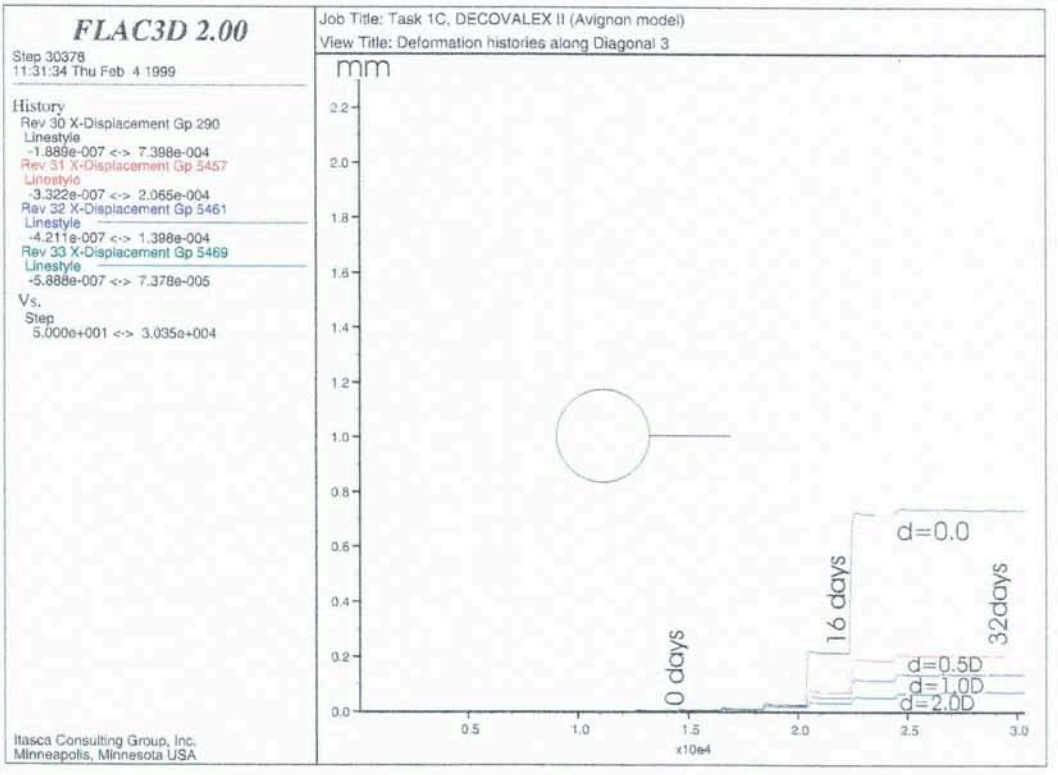

Figure 5-10 Deformation histories along Diagonal 3(σ_{Hmin} direction) at four points spaced distances from the shaft wall as given in caption of Figure 4-5.

Convergence of the shaft along Diagonal 3 together with the contours of displacement are also shown on Figure 5-12. For an explanation concerning the form of the convergence curves, see section 4.3.4.

Figure 5-13 shows the variation of the radial (σ_r) and the tangential stress (σ_t) during the excavation of Sector 7. The data are collected from a grid zone centroid closest to the nominal point P1 on the shaft wall. Here again the step-wise form of the curves illustrate the fact that the numerical excavation of each blast round was performed with no time elapsed. Figure 5-14 shows similar curves for a data collecting point closest to nominal point P3 on the shaft wall.

Figure 5-15 shows the distribution of the tangential and the radial stresses around the shaft at the depth of 660 meters. According to NIREX, the plots should include magnitudes of theses stresses that correspond to the four nominal points on each of Diagonals 1 and 3 , the points being spaced on the shaft wall, 2.7 m, 5.4 m and 10.8 m from the shaft wall. In *FLAC*^{3D} the the stresses associated with each grid zone are calculated at the centroid of that zone. Therefore the grid zones that their centroids lied closest to the nominal points produced the tangential and radial stresses needed for the plots.

On the figure, the magnitudes of the in-situ stresses, σ_{Hmax} and σ_{Hmin} are indicated with straight lines, in order that stress concentration can readily be compared with the in-situ principal stresses. Stress distributions shown on the figure are calculated when the shaft had reached the 680-meter level under the general steady state condition. As was expected, the largest concentration of the tangential stress, σ_t , occurs at the shaft wall on Diagonal 3, and its magnitude reaches as large as about two times the *in-situ* major principal stress, σ_{Hmax}.

Clearly, the disturbances of the *in-situ* stress field, as a result of the shaft sinking, extend beyond the distance of 10.8 meters (2 × shaft diameter) from the shaft wall. The disturbances presumably reach a distance of about 3 × shaft diameter (16.2m), beyond which the induced stress changes are insignificant.

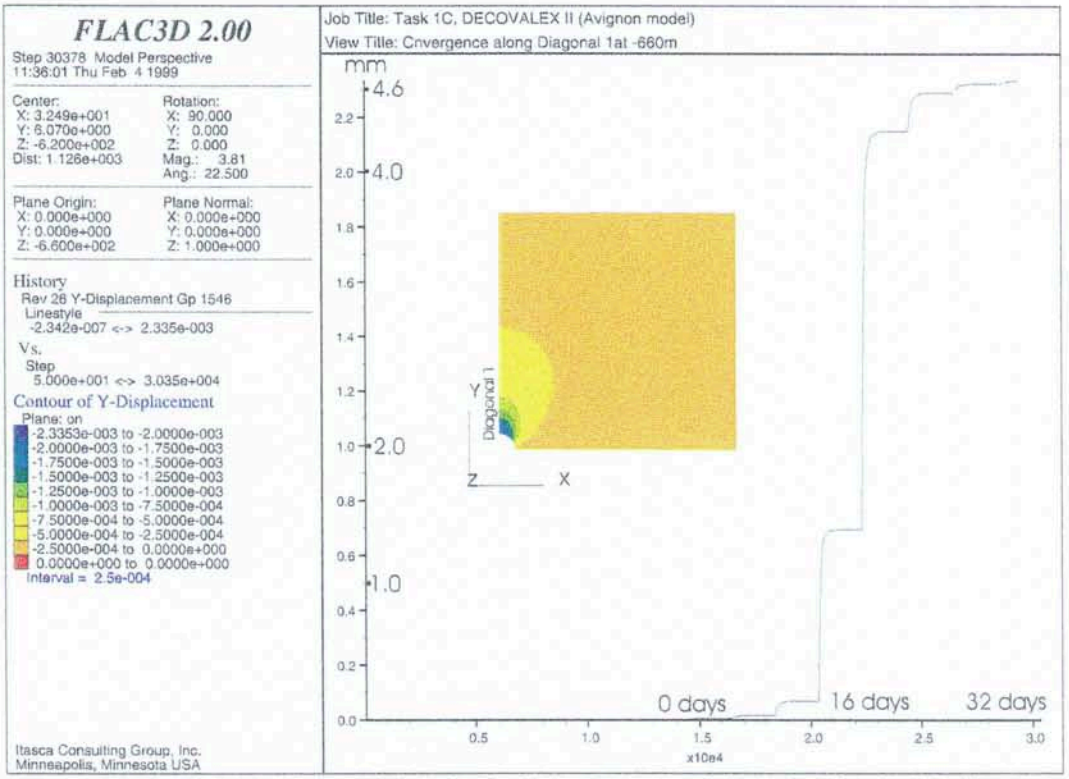

Figure 5-11 Convergence of the shaft along Diagonal 1 at the depth of 660 m. Contours of the displacement component along the σ_{Hmax} direction on a horizontal plane at that depth are also shown.

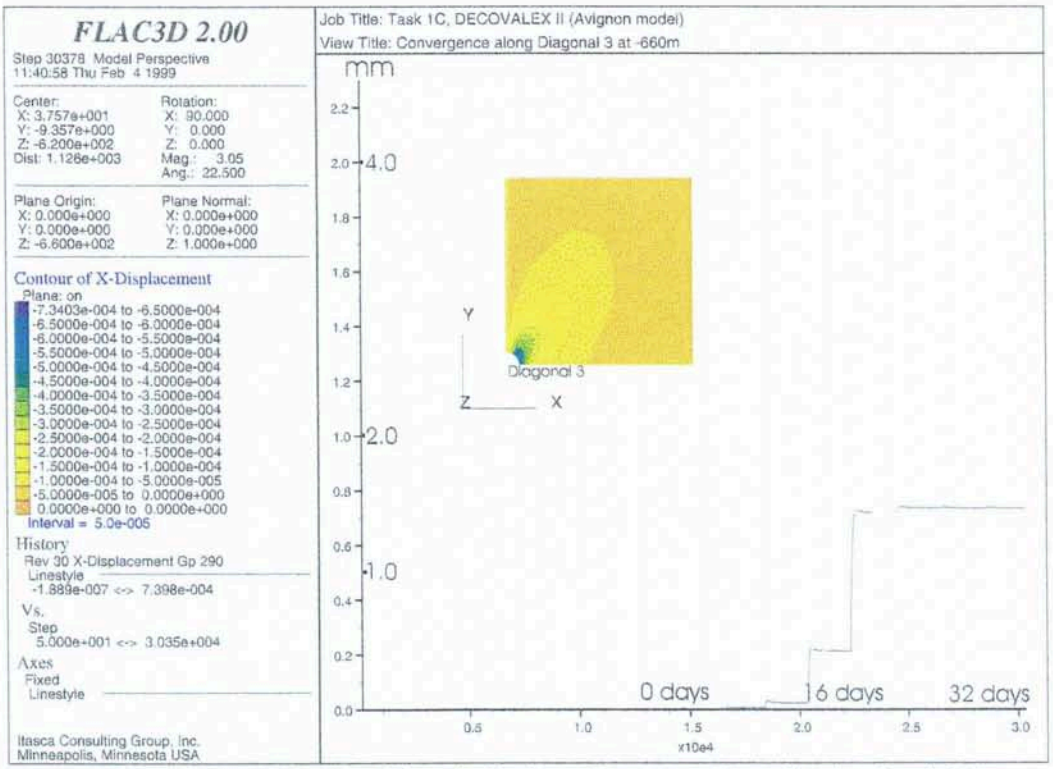

Figure 5-12 Convergence of the shaft along Diagonal 3 at the depth of 660 m. Contours of displacement component along the σ_{Hmin} direction on a horizontal plane at that depth are also shown.

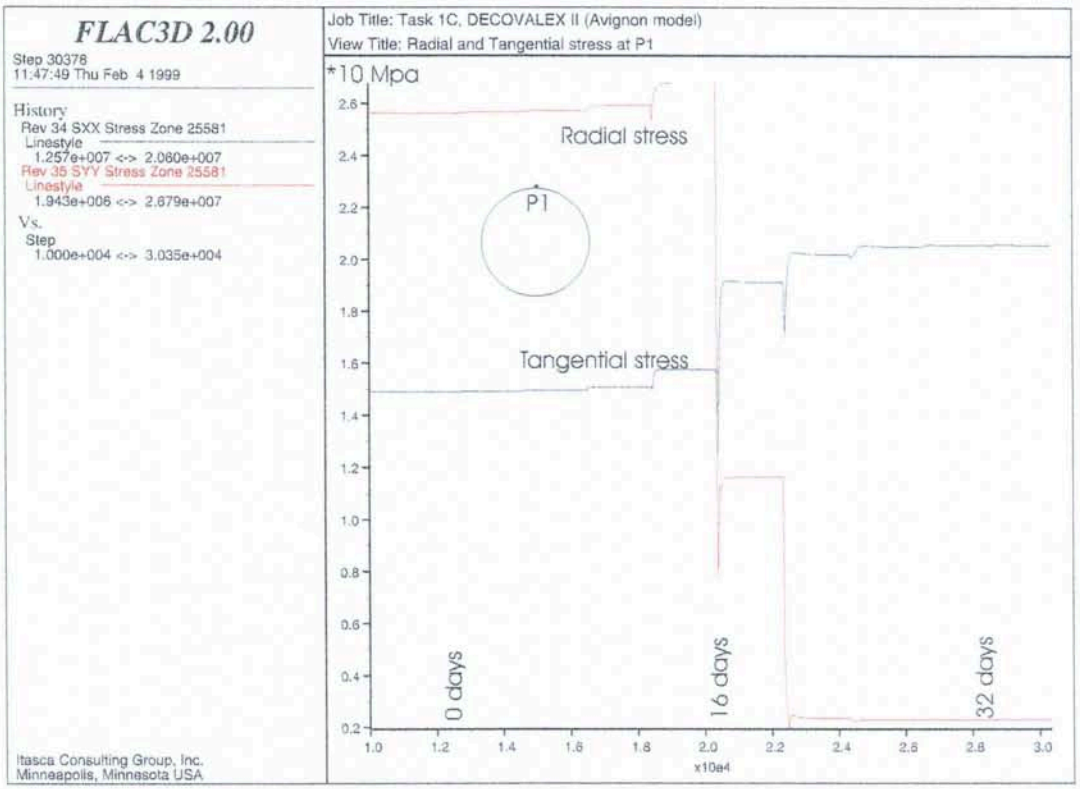

Figure 5-13 The variation of the radial and the tangential stress during the excavation of Sector 7, at the nominal location P1. Data collected from 660 m depth.

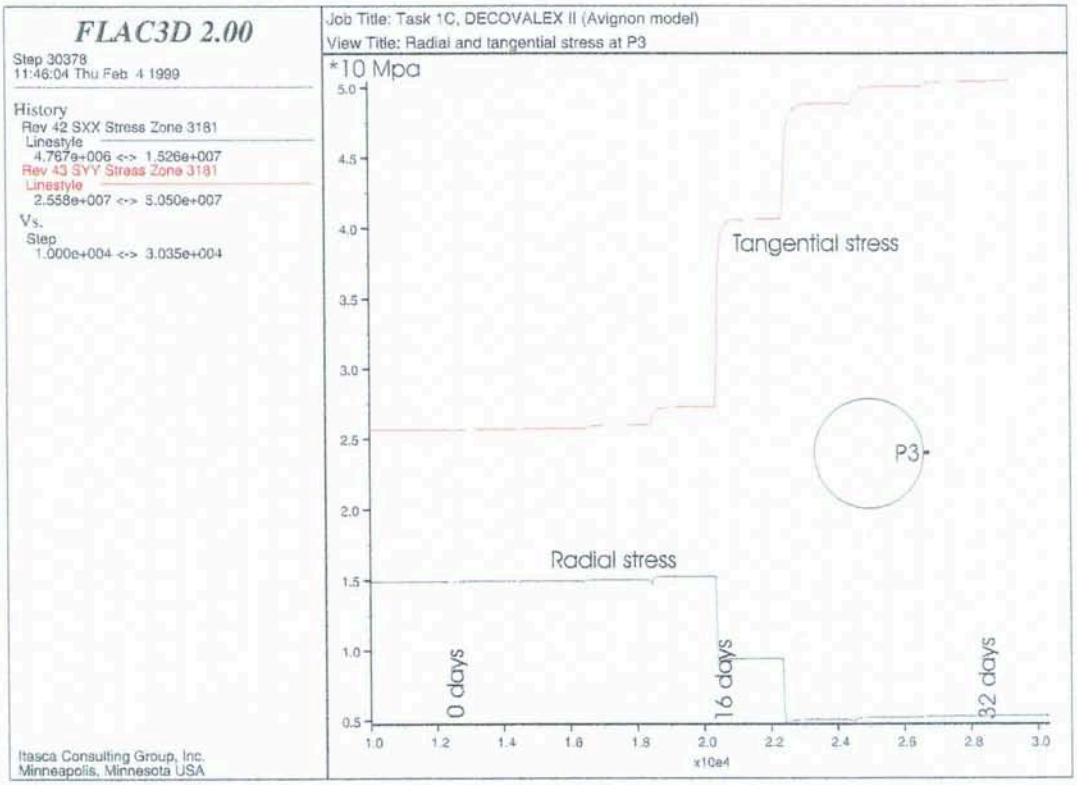

Figure 5-14. The variation of the radial andthe tangential stress during the excavation of Sector 7, at the nominal location P3. Data collected from 660 m depth.

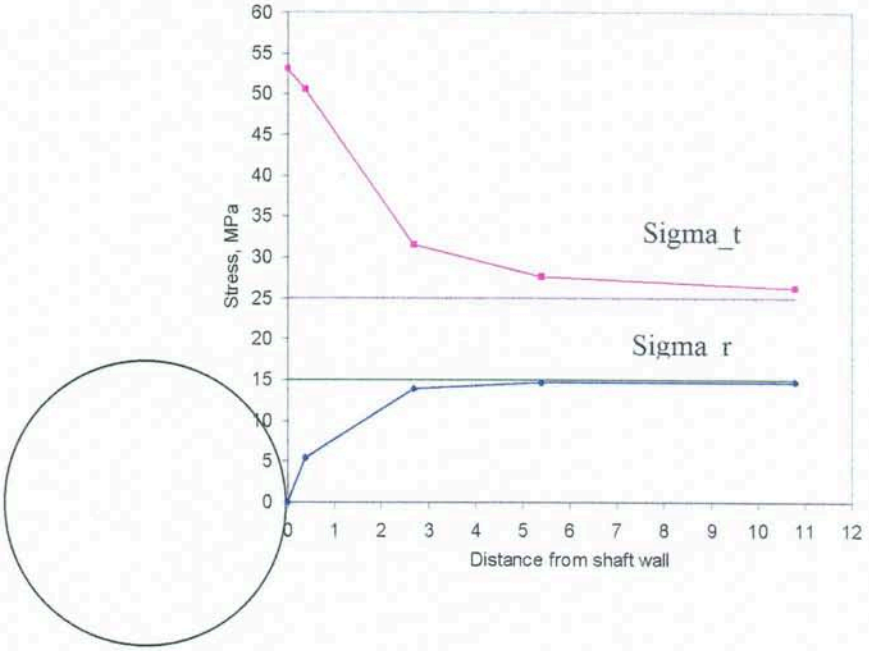

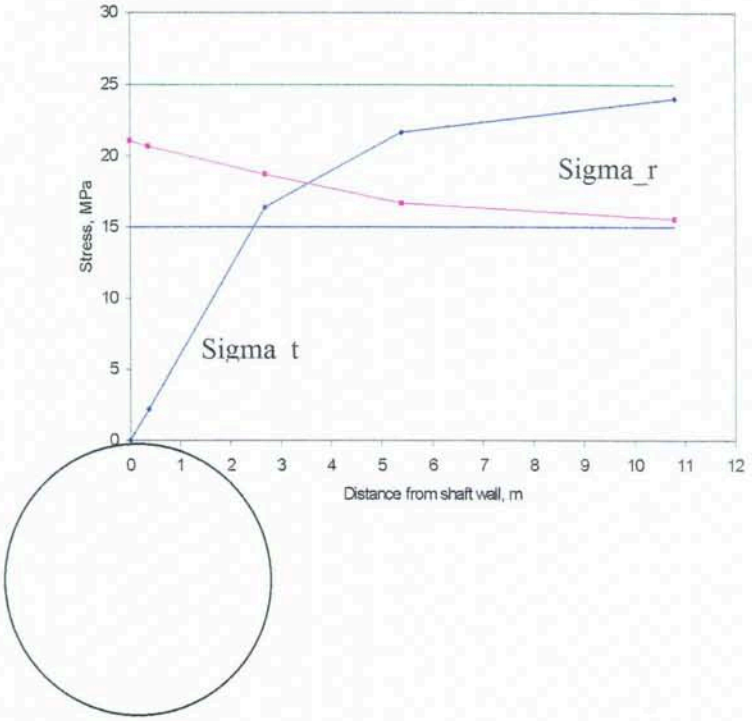

Figure 5-15 Distribution radial and tangential stress as a function of distance from the shaft walls. Data are collected from a depth of 660 m

Figure 5-16 shows the model block for mechanical computations with the majority of the grid zones closest to the shaft being failed. Note a limited number of the zones that have remained unfailed. The failed grid zones delineate the excavation damage zone around the shaft.

Figure 5-17 shows a section of the model block for the mechanical computations containing the Sector 7 (640-680 m) of the shaft. Here the number of failed grid zones have decreased in comparison with those from the upper part of the shaft. The less intensive damage zone captured in this section may be considered as more representative of what would occur in reality. This is because Sector 7 was numerically excavated in intervals of 5 meters whereas the upper part of the shaft was taken out in only two parts; 425 to 600 m and 600 to 640 meters deep.

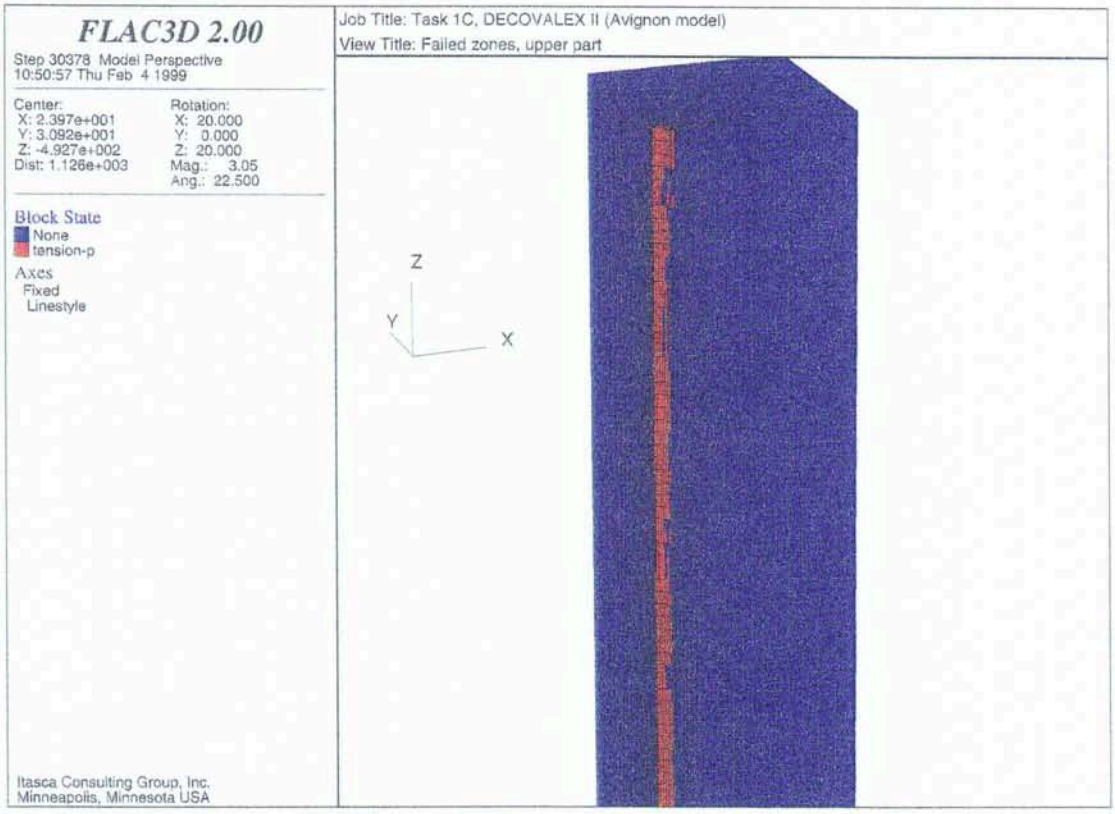

Figure 5-16 Model block for mechanical computations showing the failed zones closest to the shaft. The failed grid zones delineate the Excavation Damage Zone.

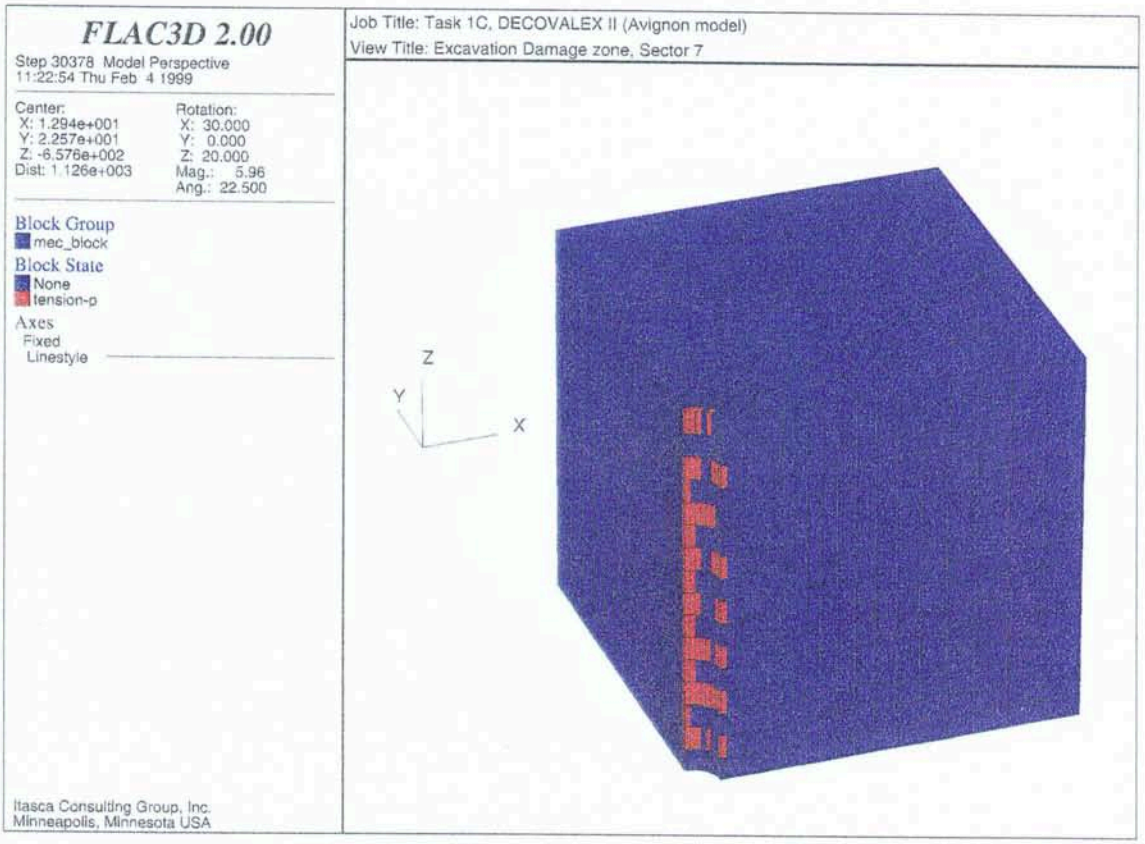

Figure 5-17 Model block for mechanical computations showing sector 7 (640 – 680 m deep) of the shaft. The failed grid zones delineate the Excavation Damage Zone.

5.4 The hydrogeological computations

5.4.1 Boundary conditions

The hydrogeological boundary conditions were the same as for the Berkeley model, see section 4.4.1.

5.4.2 Hydrogeological properties of the rock mass

Figure 5-16 shows a statistical distribution of hydraulic conductivities in the rock matrix and flow zones, interpreted by Jaimez Gomez, 1998 from the field measurements.

The selected hydraulic conductivities from the distribution shown together with other relevant parameters are given in Table 5-2 below.

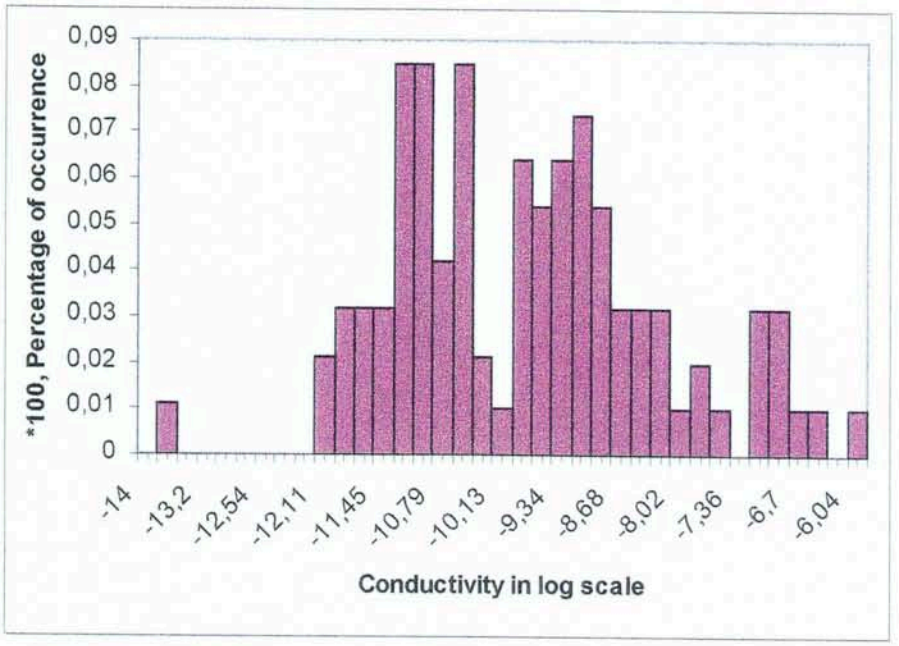

Figure 5-18 Stochastic distribution of hydraulic conductivities in the rock matrix as well as in the flow zones, interpreted by Jaime Gomez, 1998.

Table 5-2 Parameters used in hydrogeological computations

Parameter	Rock matrix	Flow zone
Hydraulic conductivity	1×10^{-10} m/sec	1×10^{-7} m/sec
Porosity	0.8%	4%
Fluid density	1000 Kg/m^3	1000 Kg/m^3
Fluid modulus	2×10^9	2×10^9

5.4.3 The sequence of computations

5.4.4 Results

Figure 5-19 shows the contours of the pore pressure throughout the model block. The front half of the block has been removed in the figure to reveal the shape of the contours inside the block.

Figure 5-20 shows the pore pressure drawdown within bore holes RCM1 and RCM2. Data have been collected at 640 m as well as at 680 m deep. The first part of the curves corresponds to the removal of rock inside the shaft from 600 to 640m deep. Four curve segments that follow show the pressure drop related to the four, 10-meter intervals of the shaft within Sector 7 removed.

Figure 5-21 shows the inflow into Window1. Inflow here includes the inflow both from the walls as well as the bottom of the shaft at any section excavated. The data collection has been extended to also show the reduced inflow into Window 1 while the excavation of Window 2 progressed. Note that the inflow into the lower section of Window 1(650 – 660m) is reduced compared with that of the upper section (640 – 650m). This is because of the location of the flow zones that run closer to the upper section of Window1.
Figure 5-22 shows the inflow into Window 2.

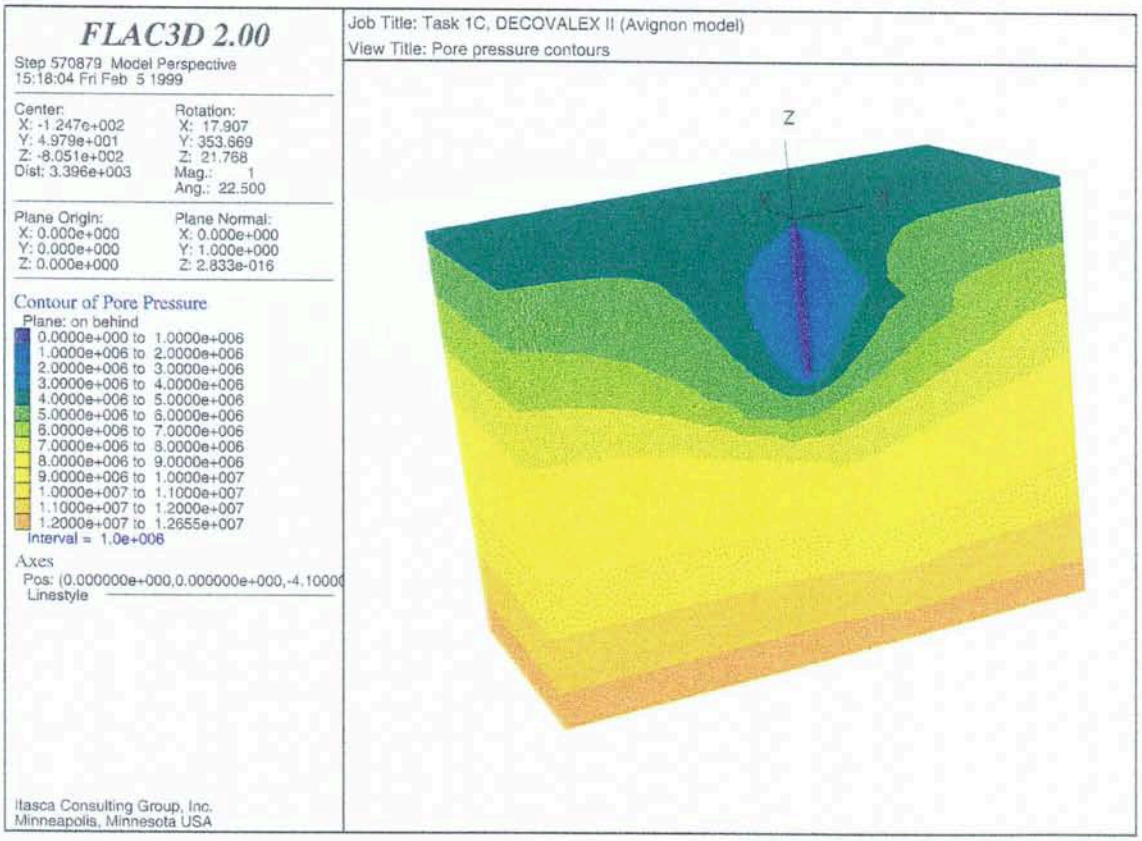

Figure 5-19 The contours of pore pressure after steady state flow has been reached at Z= 680. Only the rear half of the block is shown on the figure.

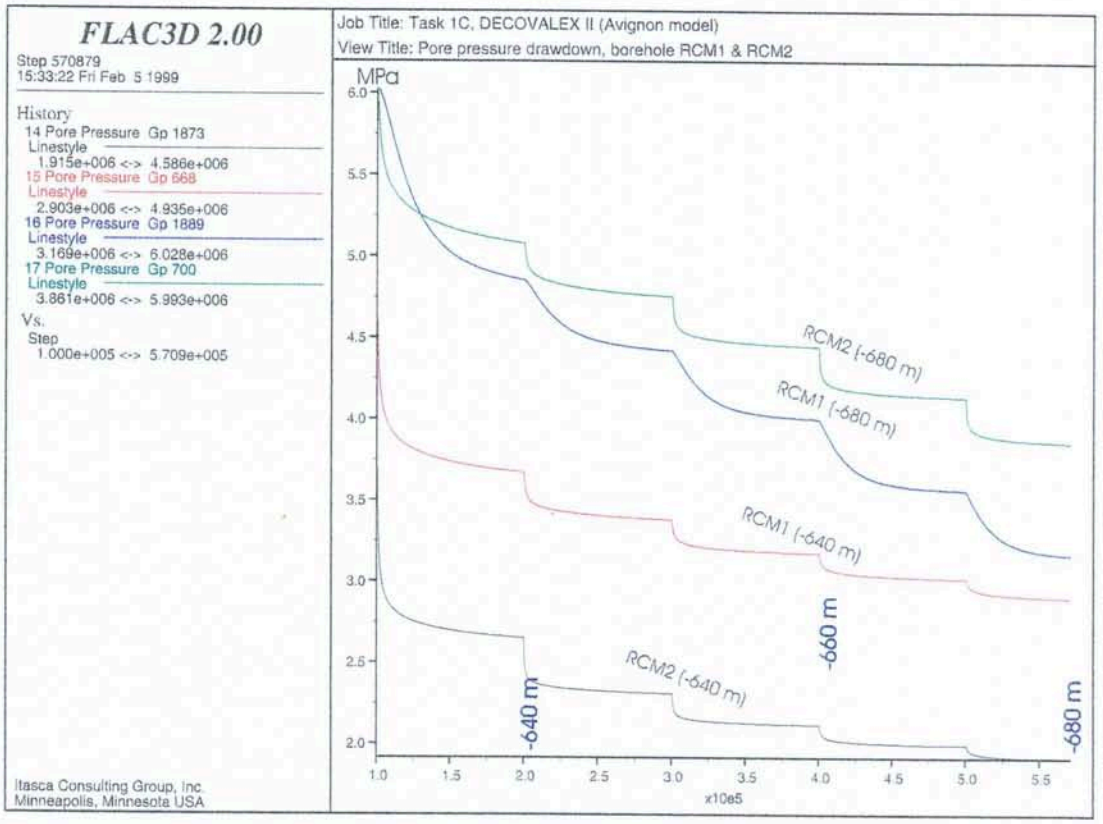

Figure 5-20 Pore pressure drawdown within boreholes RCM1 and RCM2. Data were collected from 640 and 680 m deep.

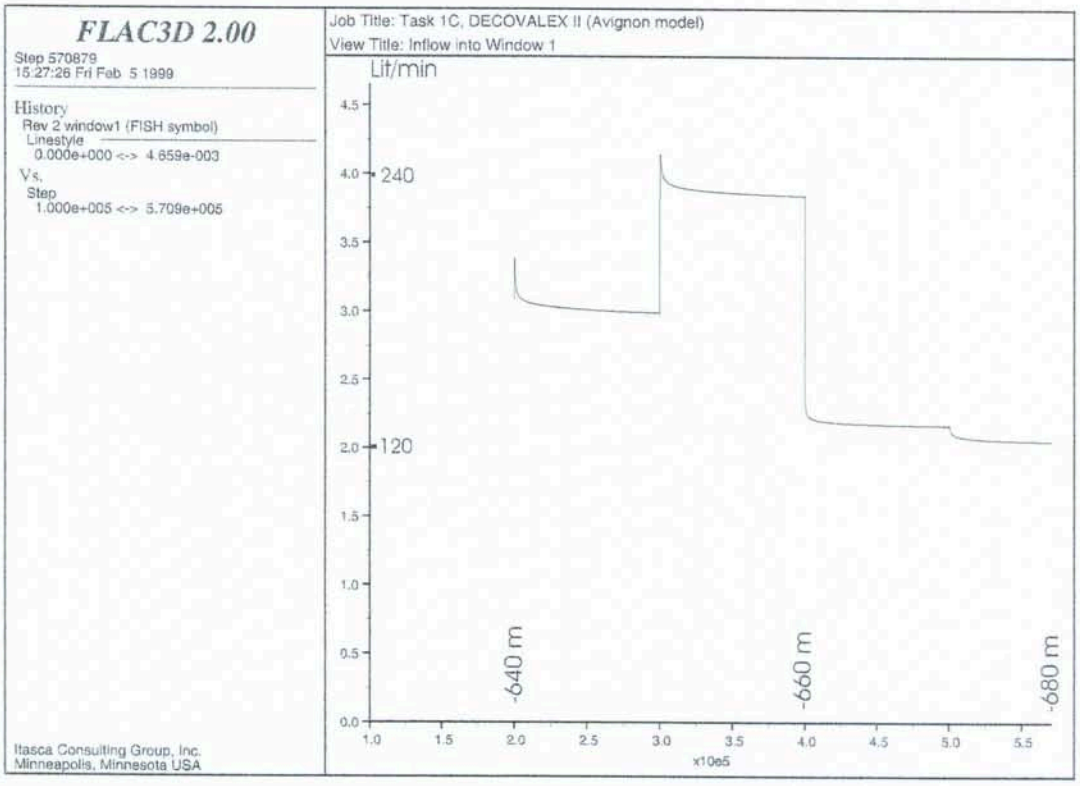

Figure 5-21 Inflow into window 1(640-660 m). Inflow is meant here to take place from both the walls as well as the bottom of the window.

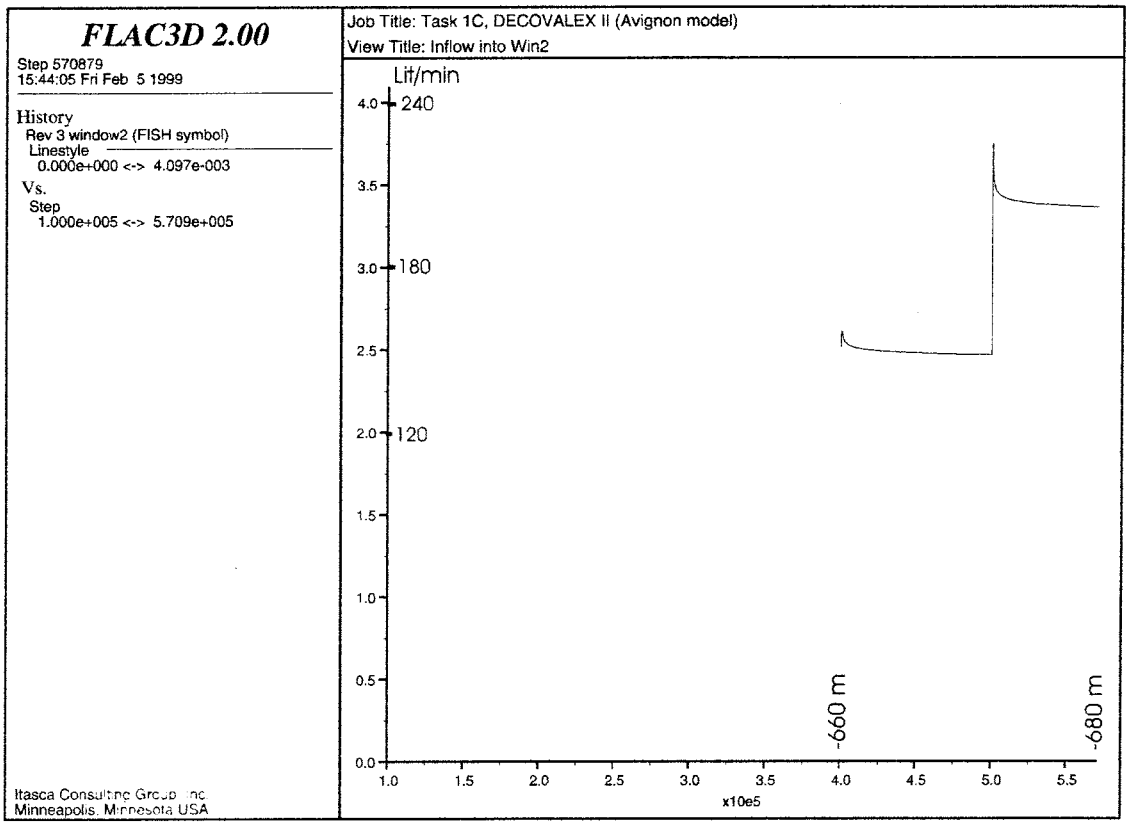

Figure 5-22 Inflow into Window 2 (66-680 m). Inflow is meant here to take place from both the walls as well as the bottom of the window.

6 Discussion

The physicochemical environment of geologic systems is host to natural chains of coupled thermal, hydraulic and chemical processes that take place continually at varying rates depending on the nature and strength of the sources of driving energies available to the systems. Man-made perturbations of the systems can affect these processes and sometimes induce undesirable events. A high-level nuclear waste repository, is considered to be a large-scale perturbation, the effect of which depends on proper understanding and assessment of the coupled phenomena that are being altered or induced (Noorishad and Tsang, 1996).

Leaving aside the chemical processes, a doubly coupled phenomena, formed of individual mechanical and fluid flow processes may be considered within the framework of Task 1C. Well known phenomena in soils, such coupling has even been observed in hard rocks (see for example Evans,1966 and Snow, 1968). Snow (1968) reported strains of 10^{-7} to 10^{-8} at a distance of about 91 m from a water well in metamorphic rocks subjected to 9 meters of drawdown.

In the structure of the continuum media, where the fractured rock is represented by an equivalent continuum model material; and as long as the induced deformations within the saturated porous medium are not of such magnitudes to cause failure (i.e. the coupling remains in the domain of poro-elasticity); the closure of the fractures in the natural rock mass, would mean a general decrease in porosity for the equivalent model material. For hard rocks as modelled, such marginal reduction in porosity would not lead to any significant change in the fluid flow characteristics.

For our specific problem, it was noticed that the effective mechanical disturbance did not extend beyond a distance of 3 times the shaft diameter, i.e. about 16.2 m. Any influences from thehydro-mechanical coupling, that could have resulted from, were judged to be, statistically, of no significance. Mechanical as well as hydrogeological processes were, therefore, investigated independently in the numerical analyses described in this report.

Inherent in the early formulating of Task 1C was the idea that the findings should be validated / calibrated against the measurements from the shaft construction, over a possible frame of time. Such validation / calibration would make it possible to better investigate the need for, e.g., the cement injections to inhibit the inflow of water into the shaft, the amount and the type of the reinforcements to put in to secure the stability

The decision to construct the shaft, however, was overruled by a political undertaking shortly after the work on Task 1C had begun. In spite of such decision, the research teams and the funding organisations were encouraged to carry on and complete the task.

Not only the lack of the field measurementsafter the excavation did not impair the quality of the investigations, it helped the nature of the problem come closer to the actual situations. In the context of the deep disposal of radioactive wastes, by an actual

situation it is meant here a situation where site investigations in combination with numerical/analytical analyses should help selecting or abandoning of a site for the purpose mentioned. The tools for numerical analyses as well as the constitutive equations planted into, should, therefore, be developed in such a way torender predictions on the long term behaviour of the rock mass in question,based on which site selection may be possible. achieve the goal described above. The fact that many of the potential instabilities of such underground facilities or hydro-thermal disturbances growing deep into a rock mass, take place over extremely long periods of time supports the idea about the role of the numerical investigations given above. Short term monitoring and measurements are, therefore, inconclusive, but help the evolution of the constitutive models that predict the long term behaviour of the rock mass.

Excavation of an underground opening in rock normally leads to a disturbed zone, a part of which in the immediate vicinity of the opening may be called the damaged zone, as it suffers much more damage in relation to the rest of the disturbed zone.

It was noticed that by changing the failure criterion, from the commonly used Mohr-Coulomb or Hoek & Brown to a modified version of those criteria, e.g. the Martin criterion (Martin, 1998), it may be possible to capture the damaged zone around the shaft in question event though a continuum mechanics approach was used. The Size of the captured damage zone captured in this way is, however, dependent on the fineness with which the grid is discretized.

Yet it remains to work out how the findings from the fairly recent field investigations aimed at characterizing an induced damaged zone could be interpreted such that they can be used as input data in numerical models.

Studies on excavation damage zone performed at Äspö hard rock library by acoustic emission measurement technique (Äspö hard rock laboratory, 1998), have indicated that an intensive microcracking occurs within the immediate vicinity of the opening, which may have the potential to be transformed into macroscopically detectable cracks. Larger permeabilities have been observed within this zone.

It has been concluded that the role of the Excavation Damage Zone as a preferential pathway to radionuclide transport is limited to the damaged zone itself. It remains, however, to study what the influence of heat, that emanates from the canisters, would be on further changing the characteristics of the damaged zone and its surroundings. It would, therefore,be important to include the heat in studies of the damaged / disturbed zones.

7 Conclusions

Within the frame for the common simplifications indispensable to any numerical modelling of a rock mass - and those made in particular to set up the models described in this report - no coupling between the mechanical and the fluid flow computations was deemed necessary.

In the domain of the mechanics of a continuum, it was shown that the numerical computations carried out by using FLAC^{3D} could produce results that corresponded well to the majority of inquiries set up under Task 1C.

By using a special programming language (FISH) that makes it possible to access the internal structure of the FLAC^{3D} code, special functions were worked out, by which the measurements of inflow into the shaft at the selected sections could be carried out.

The mechanical disturbances, assessed by studying the changes in stresses and the displacements, were typical for hard and competent rock masses. As long as the conventional Mohr-Coulomb criterion describing the rock mass strength was the basis for exposing any failure, however, no failure took place around the shaft.

A new failure criterion (Martin, 1997), that has been emerged from both the Mohr-Coulomb and the Hoek&Brown criteria, was incorporated in the simulations of the mechanical effects. By employing the criterion, which can take care of the onset of the brittle failure - in comparison to its original criteria - more explicitly, a partially failed zone in the immediate vicinity of the shaft was captured. The depth of the partially failed zone is a measure of the Excavation Damage Zone that is produced while the shaft was being excavated.

The fact that the numerical excavation of each round within sector 7 of the shaft takes place instantaneously influences both the mechanical as well as the hydrogeological results. numerical procedures are, therefore, to be worked out in order to compensate for such numerically-induced effects.

Introduction of flow zones with enhanced hydrogeological properties in an otherwise hydraulically homogeneous and isotropic rock matrix enables us to obtain rough estimates of higher possible magnitudes of inflow into the selected sections of the shaft.

As long as there would be lack of adequate information on the hydraulic characteristics of the geological boundaries surrounding the modelled volume of rock, constant head boundaries – that produce higher volumes of inflow into the shaft – are to be preferred in order to be on the safe side.

8 References

Armitage, P. D. Holton, N. L. Jefferies, B. J.Myatt and P. M Wilcock (1995). "Groundwater flow through Fractured Rock at Sellafield", AEA Technology, Report AEAT-0024, Oxfordshire, England.

Bieniawski, Z. T. (1976) Rock Mass Classification in Rock Engineering. Proc. Symposium on Exploration for Rock Engineering, Johannnesburg, Vol. 1, pp. 97 – 106.

Evans, D. M. (1966). The Denver area earthquake and Rocky Mountain Arsenal Well. Mt. Geol., 3(1), pp 23-26.

Grimstad, E. and R. Bhasin (1997). "Rock Support in Hard Rock Tunnels under High Stress. Proc. Int. Symp. On Rock Support – Applied Solutions for Underground Structures. Lillehamer (edited by E. Broch , A. Myrvang and G. Stjern), pp 504 – 513. Norwegian Society of Chartered Engineers, Oslo.

Hoek, E. (1990) Technical Note – Estimating Mohr-Coulomb Friction and Cohesion Values from the Hoek-Brown Failure Criterion. Int. J. Rock Mech. Min. Sci & Geomech. Abstr. Vol. 27, No 3 pp 227-229.

Hoek, E. and E. T. Brown (1980). Underground Excavation in Rock. Inst. Of Mining and Metallurgy, London.

Israelsson, J. (1997). DECOVALEX II RCF3 Task 1A, Pump Test Initial Predictions", Report, Itasca Geomekanik AB.

Israelsson, J. (1997). DECOVALEX II rcf3 Pump Test, Task 1B: Calibrated Flow Analyses.Report, Itasca Geomekanik AB.

Itasca Consulting Group Inc (1997) *FLAC*^{3D} – User's Manual, Minneapolis, Minnesota.

Knight, j. L. (1996). "Task 1A – Coupled Hydromechanical Effects of the Borrowdale Volcanic Group (BVG) in Response to the RCF3 Pump Test", Nirex proposal to the DECOVALEX secretariat.

Martin, C. D., 1997. Sventeenth CanadianGeothecnical Colloquium: The effect of cohesion loss and stress path on brittle rock strength. Can. Geotech. J., 34(5):698-725.

Noorishad, J. And C.-F. Tsang (1996). Coupled thermohydroelasticity Phenomena in Variably Saturated Fractured Porous Rocks – Formulation and numerical Solution. O. Stephansson, L. Jing and C.-F. Tsang (Editors) Coupled Thermo-hydro_Mechanical Processes of Fractured Media, Developments in Geotechnical Engineering, Vol. 79, Elsevier Science B. V.

Snow, D. T.(1968). Fracture deformation and changes of permeability and storage upon changes of fluid pressure, Q. Colo. Sch. Mines, 63(1), 201.

Stille, H., Groth, T.and A. Fredriksson (1982) FEM-analys av bergmekaniska problem med JOBFEM. BeFo rapport 307:1/82.

Sutton, S., R. Soley, R. C. Chackrabarty and R. McLeod (1996). "Cross hole Hydraulic Testing Between Deep Boreholes 2 and 4 at Sellafield". EUR 16967.

UK NIREX Ltd (1993) "The geology and Hydrogeology of the Sellafield Area, Volume 3, The Hydrogeology", Report No. S795/007.

Acknowledgement

This project was fully financed by the Swedish Nuclear Waste Management Company (SKB). Christer Svemar, SKB, is acknowledged for his support throughout the course of this project.

Stig-Olof Olofsson, Itasca Geomekanik AB, co-worked on the project and worked out routines for specific numerical flow computations needed. Discussions with Eva Hakami, IGAB, and her comments on the final version of the report were valuable. Viewpoints, comments and pieces of information received from other research teams working on Task 1C were useful.